Analysis of Measured and Predicted Acoustics from an XV-15 Flight Test

D. Douglas Boyd, Jr.
Casey L. Burley

Aeroacoustics Branch
NASA Langley Research Center
Hampton, VA.

Abstract

Flight acoustic and vehicle state data from an XV-15 acoustic flight test are examined. Flight predictions using TRAC are performed for a level flight (repeated) and four descent conditions (including a BVI). The assumptions and procedures used for TRAC flight predictions as well as the variability in flight measurements, which are used for input and comparison to predictions, are investigated in detail. Differences were found in the measured vehicle airspeed, altitude, glideslope, and vehicle orientation (yaw, pitch and roll angle) between each of the repeat runs. These differences violate some of the prediction assumptions and significantly impacted the resulting acoustic predictions. Multiple acoustic pulses, with a variable time between the pulses, were found in the measured acoustic time histories for the repeat runs. These differences could be attributed in part to the variability in vehicle orientation. Acoustic predictions that used the measured vehicle orientation for the repeat runs captured this multiple pulse variability. Thickness noise was found to be dominant on approach for all the cases, except the BVI condition. After the aircraft passed overhead, broadband noise and low frequency loading noise were dominant. The predicted LowSPL time histories compared well with measurement on approach to the array for the non-BVI conditions and poorly for the BVI condition. Accurate prediction of the lift share between the rotor and fuselage must be known in order to improve predictions. At a minimum, measurements of the rotor thrust and tip-path-plane angle are critical to further develop accurate flight acoustic prediction capabilities.

Presented at the American Helicopter Society 57th Forum, Washington, DC, May 9-11, 2001. Copyright ©2001 by the American Helicopter Society, Inc. All rights reserved.

Symbols

BPF	blade passage frequency
BVI	blade-vortex interaction
BWI	blade-wake interaction
dB	decibel
Hz	Hertz [sec^{-1}]
i	nacelle tilt angle [$^\circ$]
kHz	1000 Hertz [sec^{-1}]
LowSPL	SPL for $\leq$ 5 BPF [dB]
M	flight Mach number
MidSPL	SPL for $>$ 5 BPF and $\leq$ 40 BPF [dB]
P_1	measured acoustic pressure [Pa]
P_2	normalized acoustic pressure [Pa]
OASPL	overall sound pressure level [dB]
r_1	distance to microphone [ft]
r_2	normalizing distance [ft]
SPL	sound pressure level [dB]
t	time coordinate [sec]
T_1	measured period [sec]
T_2	de-Dopplerized period [sec]
V	aircraft velocity [kts]
γ	glide slope [$^\circ$]
θ_e	acoustic emission angle [$^\circ$]

Introduction

Tiltrotor aircraft, which take off and land vertically like a helicopter and fly like conventional airplanes during cruise, provide a potential alternative means of civilian transportation that could increase airport capacity without consuming large tracts of land. However, for tiltrotor aircraft to be a successful component of the civil aviation market, they must be perceived by the public as an acceptably quiet, safe, and economical mode of transportation. The noise impact of these aircraft, particularly during descent into airports, has been identified as a barrier issue for civil tiltrotor acceptance by the public. The Short Haul Civil Tiltrotor SH(CT) Program under the Advanced Subsonic Transport (AST) initiative was tasked to address the critical issues that would enable the acceptance of the civil tiltrotor aircraft [1]. Under the SH(CT) program a number of flight and wind tunnel tests have been conducted to investigate and demonstrate advanced technologies related to civil tiltrotor aircraft. To date, flight tests have focused mainly on the examination of safe, low-noise terminal area operations and noise abatement procedures for approach operations [2, 3, 4, 5]. Results from these test are usually presented as a comparison of several noise metrics for the various conditions flown. Wind tunnel tests have focused primarily on determining the basic aerodynamic and aeroacoustic characteristics of different proprotor designs [6, 7, 8, 9].

In addition to the experimental work, tiltrotor aeroacoustic prediction methodologies were, and continue to be, developed. One such prediction methodology developed under SH(CT) is the TiltRotor Aeroacoustic Code (TRAC) system [10, 11, 12, 13, 14]. TRAC's objective is to provide analysis for evaluation and design of efficient, low-noise tiltrotors and to support the development of safe, low-noise flight profiles. To date, the primary focus in the TRAC system has been on methodology development based on isolated rotor wind tunnel tests. Recently, however, high quality flight data have become available and preliminary comparisons between measured and predicted data have been made [15, 16]. Initial TRAC predictions for an XV-15 tiltrotor were presented by Prichard [15]. In this paper, a more detailed examination of XV-15 flight data is made, and the relationship of that data to requirements of prediction efforts is outlined.

This paper is divided into three parts. The first part discusses the prediction methodology and assumptions typically used in TRAC. The second part presents an analysis of the measured data for several flight conditions. Quantities examined include aircraft state data, acoustic pressure time histories, and integrated noise metrics. The third part presents comparisons of predicted and measured data for nominal and off-nominal conditions.

Prediction Methodology

The aeroacoustic calculations presented in this paper were made using the TRAC prediction system. This system consists of a collection of computational fluid dynamic (CFD) and non-CFD based computer codes, developed over the past decade to compute aerodynamics, dynamics, performance, wakes, and acoustics for rotorcraft. For this paper the non-CFD option of TRAC is utilized and shown schematically in figure 1.

In brief, the prediction method trims the vehicle forces and moments to specified flight conditions using CAMRAD.Mod1. High resolution far wake velocities are computed using HIRES, which are then used to determine the high resolution rotor airloads using the Indicial Post Processor (IPP). These rotor airloads are then used by the acoustic analysis WOPMOD to predict the noise at specified locations. Details of each of the analysis codes can be found in the literature. Burley, *et al.,* [14] lists a comprehensive set of references for TRAC prior to September 1999. Since then, several other references have appeared in the literature [15, 17]. The analysis codes in figure 1 will be discussed here only briefly to highlight assumptions that affect flight correlations.

CAMRAD.Mod1 is a highly modified version of the original Comprehensive Analytical Model of Rotorcraft Aerodynamics and Dynamics (CAMRAD) computer code [18, 19]. This version obtains the vehicle trim and performance by predicting the aerodynamics and dynamics of a two rotor aircraft (*i.e.,* tiltrotor aircraft, main/tail rotor aircraft, *etc.*). The aerodynamics of the fuselage are determined

by a table lookup based on the conditions, as are the aerodynamics of each blade. The rotor blade wakes are represented by a multi-core roll-up model and the modeling parameters used here are consistent with those used by Burley, *et al.*, [14] and Prichard [15]. For a tiltrotor, the trim procedure assumes that the flight condition is symmetric. That is, it is assumed that the behavior of both rotors is identical, but "mirror-image." In addition, it is assumed that the flight is along a non-accelerating, straight flight path. This flight path is assumed to be either a constant descent ($\gamma > 0.0$), constant climb ($\gamma < 0.0$), or level flight ($\gamma = 0.0$). The current prediction method does not allow for variation of the glideslope within a given trim condition. Non-symmetric effects such as vehicle yaw and roll angles are also not modeled in the trim. Detailed effects of the fuselage on the rotor flowfield or the rotor on the fuselage flowfield are not included. However, the aerodynamic effect of the fuselage on the rotor trim is included *via* a fuselage aerodynamics lookup table [20].

HIRES computes wake influence coefficients and velocities at high radial and azimuthal resolution for each rotor based on interpolated blade and wake locations previously computed at a lower resolution in CAMRAD.Mod1. Since HIRES is currently an extension of CAMRAD.Mod1, all of the assumptions discussed above apply to HIRES as well. The information generated by HIRES is then used in the IPP to compute high resolution airloads based on indicial response functions developed by Beddoes [21, 22], Beddoes, *et al.*, [23, 24], and further developed at NASA Langley [13]. These high resolution airloads are then used to compute the rotor tone noise using the WOPMOD code. WOPMOD is a modified version of WOPWOP [25] which incorporates direct input of blade motion, flight condition, and aerodynamics from CAMRAD.Mod1, HIRES, and IPP output files. WOPMOD is designed to use only one rotor. Since a tiltrotor is a two rotor vehicle, and since the trim procedure assumes symmetric flight and rotor conditions, WOPMOD can be executed in two ways. The first possibility is that it can be executed for one rotor only, and the results summed using a symmetry condition at each observer. The second possibility is that WOPMOD be executed twice, once for each rotor and the results from each rotor summed at each observer. For a truly symmetric flight condition, both possibilities yield the exact same answer. Typically, the first possibility is used regardless of the flight condition.

The acoustic predictions include tone noise only. Broadband noise sources such as blade-wake interaction (BWI) [26, 27], rotor self noise [26], engine noise, and airframe noise are currently not included. Acoustic reflection and refraction effects are also not included.

Due to the nature of flight measurements (*i.e.*, a non-constant glideslope, non-symmetric rotor loading, acceleration, *etc.*) many of the prediction assumptions are violated. It is not clearly understood to what extent these violations affect the accuracy of current flight prediction methods found in TRAC. To begin to understand and assess these effects, it is necessary to first examine the measured quantities in detail and determine to what extent they violate certain assumptions. The next sections provide a detailed examination of measured flight data.

Flight Measurements and Analysis

Test Description

The flight data examined in this paper are from an XV-15 acoustic flight test which was conducted in June 1995 near Waxahachie, Texas. This was a test conducted jointly by NASA, the U.S. Army, and Bell Helicopter Textron, Inc. (BHTI) under the sponsorship of the SH(CT) program. One of the main objectives of the flight test was to determine relative noise differences between the various vehicle configurations and flight conditions. The test was conducted in two phases. In Phase I, acoustic data was acquired using a linear microphone array that was perpendicular to the flight path. In Phase II, the microphones were deployed over a wide area instead of linearly. Only the data from Phase I is considered for this paper.

The XV-15 aircraft is a tiltrotor aircraft with a conventional wing-tail configuration. The two proprotors are counter-rotating and mechanically synchronized, and the rotor/engine/gearbox nacelles can be rotated from a vertical "helicopter mode" (nacelle tilt $i = 90^\circ$) to a horizontal "propeller mode" (nacelle tilt $i = 0^\circ$). The rotors have a diameter of 25 feet and are located at the wing tips

which are approximately 16 feet from the aircraft centerline. Specific design details of the aircraft, including the flight envelope, are provided in reference [28].

Flight Measurements

For each flight run, acoustic data as well as aircraft state and aircraft position (tracking) data were obtained. The test matrix included a range of nacelle tilts, airspeeds, and glideslopes (descent angles) [5].

The acoustic data were obtained during the test by flying the aircraft over a linear array of 17 ground board, flush mounted microphones deployed perpendicular to the flight path, as shown schematically in Figure 2. The microphone array is oriented perpendicular to the nominal flight path. The unequal microphone spacing was designed such that, when the aircraft is 394 feet directly over the array, the microphones are spaced at a 10° angular resolution to both sidelines [4]. For reference, microphone #9 is the centerline microphone, that is, it is directly in line with the nominal flight path. In this paper, data from microphones #9 (located on the centerline), #6 (located 227.5 feet to starboard of the centerline), and #12 (located 227.5 feet to port of the centerline) are examined in detail.

Eight test runs are examined in this paper and indicated in Table 1. The Level Flight Runs 1-4, are repeat runs of the same flight condition and the other four runs are constant descent conditions. The repeat runs are a special flight condition known as a "housekeeping run," which were repeated seventeen times, at least once during each flight run to verify functionality of the equipment. The "housekeeping run" is a level flight condition ($\gamma = 0^\circ$) with the nacelle tilt of 60°, nominal airspeed of 90 knots and an aircraft altitude of 394 feet. Both the roll and yaw angle of the aircraft are also nominally zero degrees. The flight test log (Appendix C of reference [5]) documented comments from the pilot and test team about every run of the test. The comments indicated that not every "housekeeping run" was considered successful. A number of the runs were aborted for various reasons and some of the runs had incomplete data sets. Hence only 4 out of the 17 runs were found to contain a complete set of data and no adverse comments.

Description	XV-15 Flt # / NASA Run #	V [kts]	i	γ
Level Flight 1	171a/175	90	60°	0°
Level Flight 2	171b/185	90	60°	0°
Level Flight 3	173a/201	90	60°	0°
Level Flight 4	173b/212	90	60°	0°
3° Descent	162/127	90	60°	3°
6° Descent	171a/181	90	60°	6°
9° Descent	168b/154	90	60°	9°
9° Descent BVI	168a/148	70	85°	9°

Table 1: Nominal run conditions for XV-15 flight data.

Even though each of these "housekeeping runs" were intended to be identical, significant variations between the repeat runs and significant variations from the nominal condition were observed due to "real world" factors. Since prediction analyses typically assume that variation in these parameters is zero, the effect of the measured variations on predicted acoustics is assessed. Specifically, variations in the aircraft airspeed, yaw, pitch and roll angles, altitude and glideslope are examined in detail. Unlike wind tunnel testing, the number of parameters that can be directly controlled is much more limited for flight testing, which contributes to the difficulty in comparing flight measurements with prediction.

The four descent conditions examined include a glideslope sweep as well as a high BVI condition. The glideslope sweep consists of three descent conditions, $\gamma = 3^\circ$, 6°, and 9°, all flown with a nominal airspeed of the 90 knots, a nacelle tilt of 60°, and roll and yaw angles of zero degrees. The BVI condition was flown nominally at 70 knots with a nacelle tilt of 85° at a 9° descent angle. This is a high BVI condition, where the rotor is operating within its own wake. These descent conditions were chosen in order examine the variation in flight condition from the nominal as well as determine the effect of this variation on the resulting measured and predicted acoustics.

Aircraft State Data

An onboard recording system monitored a number of basic aircraft flight parameters and operating conditions. These parameters were recorded and stored at various sample rates, but were all time synchronized using GPS time code. For this paper, the raw onboard data was smoothed using a 3 second moving average. Since the parameters were recorded at various sample rates, after smoothing, they were re-sampled at a rate of once per revolution. In addition, the aircraft position was monitored using a laser tracking system accurate to within ± 1 foot in range and 0.1 mrad in azimuth and elevation [4].

The state data that is required for prediction include aircraft airspeed, altitude, glideslope, and aircraft orientation (yaw, pitch, and roll angles). These data are examined in detail to determine flight run repeatability and to compare the data to the nominal conditions. Figure 3 shows the airspeed for level flight runs 1 through 4. Also shown is the nominal (intended) airspeed of 90 knots. The horizontal axis is time relative to the time when the aircraft is directly over the array. Time is zero when the aircraft is directly overhead. Time is negative when the aircraft is approaching the overhead position and positive after it has passed overhead. The vertical axis is vehicle airspeed in knots, as measured from the system onboard the aircraft. It can be seen that, for all of these level flight runs, the aircraft was traveling faster than the nominal flight speed by several knots. Runs 1 and 3 have an airspeed that is relatively constant, while runs 2 and 4 have airspeed variations as much as 5 to 6 knots over the 40 second interval shown. Airspeeds for the descent conditions are shown in figure 4. The nominal 90 knot airspeed for the first three descent conditions and the nominal 70 knot airspeed for the high BVI descent condition are shown as bold lines. The 3° descent condition has a constant airspeed about 2 knots below the nominal, but the airspeed for the 6° and 9° conditions varies as much as 4 to 7 knots during the 40 second interval. The airspeed for the BVI descent condition, is within ± 2 knots of its nominal value for the 40 second interval. These variations in airspeed directly affect the loading on the rotors and the fuselage (and thus the trim state of the vehicle), which both have first order effects on the noise.

Figure 5 shows the altitude of the aircraft for the level flight runs, as measured by the optical tracking system. The bold line shows the intended flight altitude of 394 feet. All of the level flight runs are within one rotor diameter of the intended altitude. Figure 6 shows the three descent cases and the BVI descent case. Each bold line shows the intended altitude versus flight time. The intended flight paths for all the descent conditions are such that the aircraft is 394 feet above the microphone array at the overhead time. The 3° descent case follows its nominal path closely, but the 6° and 9° descent conditions vary considerably, particular for times after the aircraft has flown overhead. For the initial 5 seconds of the interval shown, the 6° descent is mirroring the 9° descent case along the 9° nominal path. Between 15 and 10 seconds before overhead, the 6° condition actually descends at an angle steeper than 9°. For the remainder of the 6° run, the angle is between 6° and 9°.

The 9° descent BVI case follows an even more variable course than the other three descent cases. It starts off at a 9° descent, but at a lower altitude than the 6° and 9° descents, then flattens out to a 6°, then to a 3° descent by the overhead time. After the aircraft passes overhead, the flight path follows the original 9° flight path. It is expected that variations of this magnitude will result in significantly different predicted trim states as well as distinctly different acoustics, particularly for a high BVI condition.

The lateral position of the aircraft, relative to the nominal flight path (which passes over the centerline microphone location) is shown in figures 7 and 8. The nominal flight path is along the zero value. For all of the flights the aircraft is within only 50 feet (two rotor diameters) of the centerline.

The measured aircraft yaw, roll, and pitch angles are given in figures 9-14. The bold lines in Figures 9-12 represent the nominal angle. The yaw angle for most of the level flight cases is relatively constant, averaging from about 3° for run 2 to about 9° for run 3. Figures 11 and 12 show the roll angles for both the level flight and descent cases are within $\pm 5^\circ$ of the nominal zero value. At the end of the 6° and 9° descent cases, the roll angle diverges. This is due to

the pilot "peeling off" and departing the area at the end of the run.

The fuselage pitch angle relative to the horizon is shown in figures 13 and 14. There is not a nominal pitch angle, since the fuselage pitch is a function of the aircraft trim condition. For the level flight conditions, the pitch varies between 2° and 5°. The same order of variation is seen for the descent cases, however the average pitch between each case varies substantially more than for the level flight cases. For the 9° descent BVI condition, the pitch is relatively constant at approximately a 4.5° nose-down attitude.

To fly a prescribed flight condition, the pilot must continuously monitor the flight state and make adjustments to maintain that condition. Hence the variations noted in airspeed, altitude, and vehicle orientation are due to the pilot maintaining a given flight condition and flight path. These variations will be shown to significantly affect the character and amplitude of resulting acoustic time histories, as well as the overall directivity of the noise.

Flight Acoustic Data

The primary focus of the 1995 XV-15 flight test was to compare acoustic footprints for various terminal area operations, such as takeoff and landing [4]. These comparisons were based on a set of A-weighted, integrated noise metrics such as the Overall Sound Pressure Level (OASPL). Examination of these integrated metrics is appropriate for comparisons of various terminal area operations. However, for assessment of capabilities of prediction tools and for understanding the underlying noise mechanisms involved, examination of acoustic time histories is essential. This can be seen specifically in the acoustic aspects of prediction work by realizing that any number of acoustic pressure time histories, or waveforms, are capable of generating the exact same OASPL. Therefore, it is more important to examine the fundamental quantities, such as the acoustic pressure time histories, rather than just the integrated quantities when assessing a prediction tool or when trying to understand the underlying physics of the noise mechanisms involved. Indeed, if these fundamental quantities are predicted correctly, the predicted integrated metrics will be correct as well.

So, the primary data of interest when comparing prediction to acoustic flight measurements, is the acoustic pressure time history. All other noise metrics can be derived from the acoustic pressure time histories, if desired. Hence, the pressure time histories will be discussed and presented in detail.

In this test, the acoustic data were acquired at a sample rate of 20kHz. Typically, when presenting flight acoustic data, ensemble averaged time histories are shown. However, in this paper, we present the unaveraged acoustic pressure time histories in order to show any blade to blade differences that may be present in the data. Furthermore, comparison of measured flight acoustic pressure time histories with prediction is complicated by the fact that the aircraft is moving relative to the microphones; both Doppler and spherical spreading effects are contained in the measured data. In order to make the comparisons between measured and predicted data more straight forward, the Doppler effect is removed from the measured data and all of the acoustic pressure amplitudes are normalized to be the same distance from the aircraft.

The Doppler effect is removed from the acoustic pressure time histories by simply scaling the period over a short time interval. The measured data time period, T_1, is changed to T_2 by the following formula:

$$T_2 = T_1(1 - M\cos\theta_e) \tag{1}$$

where M is the flight Mach number and θ_e is the acoustic emission angle. The flight Mach number is computed from the onboard measured data at the retarded time. The acoustic emission angle is determined from the aircraft position at the retarded time. This scaling assumes that both the airspeed and the acoustic emission angle are constant over that short time interval. Examination of the data indicates that this assumption is reasonable for the short time intervals considered ($T_1 \approx 0.1$ seconds).

The measured amplitudes of the acoustic pressure are normalized to a constant distance from the aircraft. The constant distance used is 394 feet, which is the nominal altitude of the aircraft when it is directly above the microphone array. The measured acoustic pressure P_1 at a distance r_1 is normalized by the following equation:

$$P_2 = P_1 \left(\frac{r_1}{r_2} \right). \qquad (2)$$

where $r_2 = 394$ feet. The normalized values are presented in the figures.

In addition to examination of individual acoustic pressure time histories, two integrated spectral metrics ("LowSPL" and "MidSPL") are also examined and presented in the form of acoustic "footprints." LowSPL represents the low frequency acoustic content and MidSPL represents the higher frequency acoustic content for which BVI noise is dominant. The computation of these two metrics is as follows. For a given flight time and microphone, three contiguous acoustic pressure time history segments, consisting of 4096 points each, are extracted from the raw data. The effect of spherical spreading is removed by applying equation (2) to the acoustic pressures. This set of three contiguous time histories, consisting of 12288 points in all, is centered on the current time at the current microphone as shown in figure 15. Based on the number of points and the sample rate of 20 kHz, each window occupies a 0.2048 second time interval, which corresponds to approximately two rotor revolutions of data. These three time segments are labeled 1, 2, and 3 in figure 15. Using the data in the three time history segments, two additional overlapping time history segments, labeled 4 and 5 are constructed. To reduce the effects of a finite length segment on the results, a Hamming window [29] function is applied to each of the five time history segments. Then, a Fast Fourier Transform (FFT) is taken to determine the spectral content of each segment. The spectra from these overlapping segments are then ensemble averaged to reduce statistical variability [30] of the spectrum. The Doppler effect is removed from the spectra by applying equation (1).

Once the spectra are computed for all flight times and all microphones, the LowSPL and MidSPL components are computed. The LowSPL metric is computed by summing all of the spectral contributions up to the 5th blade passage frequency (BPF). The MidSPL metric is computed by summing all of the spectral contributions between the 5th BPF and the 40th BPF.

Acoustic Time Histories: Housekeeping Runs

The variability of the acoustic pressures for each of the housekeeping runs is considered by examining the unaveraged acoustic pressure time histories of length 0.1 seconds. The 0.1 second time interval was chosen because it is almost exactly equal to one rotor revolution. (Actually, at the nominal 589 RPM, one rotor revolution is equal to a period of 0.1018 seconds.) Figures 16-18 show the unaveraged time histories for all four level flight runs. Both the Doppler effect and the spherical spreading effect have been removed.

Each figure, contains time histories that are sampled 5 seconds apart, ranging from 15 seconds prior to the aircraft passing over the array (labeled "15 sec prior") to 5 seconds after the aircraft has passed over the array (labeled "5 sec after"). When the aircraft is directly over the array time history is labeled "overhead." Here, the time relative to the overhead time refers to the flight time as measured by the optical tracking system, not the retarded time. Note that in all of the plots, the horizontal axes have the same time scale, which is the 0.1 second interval centered on the time relative to overhead. However, the scale on the vertical axis changes. Before the overhead time, the vertical scale ranges from -50 to 20 Pascals. At overhead and later, the vertical scale is expanded to range from -10 to 10 Pascals in order to better show the signature details.

The four housekeeping runs have similarities as well as notable differences. For all times prior to the aircraft passing the array, nearly all the acoustic signals are dominated by impulsive events that increase in amplitude as the aircraft approaches the array. Using a simple analysis based on the airspeed, altitude of the aircraft and the rotor shaft tilt, it can be shown that the microphones are in the plane of the rotor when the aircraft is 5 seconds prior to overhead. Thickness noise is generally dominant in the rotor plane and typically appears as strong negative impulses in the acoustic time history. Most of the measured acoustic pressure time histories at 5 seconds prior contain strong negative pulse(s) which are attributed to thickness noise. This is also found to be supported by examining the components of the predicted noise at these locations. It is not expected

that there would be strong BVI noise measured at this location for this level flight condition.

Even though the four housekeeping runs were intended to be identical, some of the time histories are quite different. For level flight run 3, (figure 16) for the 15, 10, and 5 seconds prior to overhead there is a large "double peak" in the signal. The double peaks are much less evident in the data from runs 1, 2 and 4. Assuming that each peak comes from a different rotor, then the time between the two pulses (multiplied by the speed of sound) is a measure of the difference in distance that the sound traveled from the two sources to the microphone. Since the aircraft is symmetric, and the microphone is on the nominal flight path centerline, then the cause of the extra distance traveled can be associated with some combination of the aircraft being laterally displaced from the nominal centerline, the aircraft being at a non-zero roll angle, or the aircraft being at a non-zero yaw angle. Based on the measured time between the pulses for run 3 at 5 seconds prior to overhead, the distance between the two sources is approximately 5 feet. This difference is well within the variability of the vehicle location during the flight runs.

To the authors' knowledge, the first documentation of these double acoustic peaks for the XV-15 was in 1987 by Brieger, *et al.*, [31]. There, for slightly different flight conditions and with the rotors configured out of phase by 4° of azimuth, they showed similar results to those presented here. They also suggested that the double peak is not related to the 4° of rotor phasing. That conclusion is supported here since there is no rotor phasing in this test, yet similar double peaks are still found.

When the aircraft is directly over the array, the signal is dominated by low frequency blade loading noise and broadband noise, which is seen as high frequency signal superimposed on the lower frequency loading noise. The negative pulse seen at earlier times is essentially nonexistent. Actually since the rotors have a nacelle tilt of 60° the microphones are not directly below (and perpendicular to) the rotor plane until the approximately one second after the aircraft is overhead. The difference between the acoustic signal at that time and overhead is negligible, but between that time and 5 seconds after overhead the low frequency loading noise decreases considerably. Once the aircraft is 5 seconds past overhead, the signal is dominated by broadband noise. The character of the broadband signal suggests that it is associated with rotor broadband noise rather than engine or airframe noise. For times later than 5 seconds after overhead, the broadband character of the signal is found to decay rapidly. Also, the impulsive character of the signal in this region is absent and has been replaced by a much smoother blade passage event with a frequency indicative of blade loading noise. Also of note is that, for any given run, blade to blade differences are very small.

These differences in the "identical" level flight conditions have implications for prediction work. It is important to be aware of the kinds and levels of differences in the measured data. For example, a common technique for prediction of a nominally level flight condition is to assume that there is a plane of symmetry. This assumption of symmetry leads to the conclusion that it is not possible to have a double peak even at the centerline microphone (as seen in figure 16, run 3). However, the measured data show that relatively small perturbations to that level flight condition can create large changes in the character of the measured acoustics (*e.g.*, having no double peak event *vs* having a double peak event).

Figures 17 and 18 are the same as the previous figure, except the data are from the symmetrically placed sideline microphones 6 and 12. The data trends are similar to those observed for the centerline microphone. However, as expected, the existence of double peaks is much more prevalent. This is in part attributed to the distance differences between each rotor and the microphone, due to the rotor orientation and as well as its location.

Comparison of the signals from microphones 6 and 12 (figures 17 and 18) show that they are quite similar to each other. The primary difference appears to be that the acoustic pressure double peaks are separated by slightly different times. By assuming that the double peak is composed of one peak from each rotor, which is supported by the similarity of the two pulses in the double peak event, it can be seen that the two rotors are generating similar acoustic signatures which arrive at the microphone at slightly different times. Furthermore, since the time between the two peaks is different between the port and starboard microphones, this indicates that the aircraft is not symmetrically oriented and is dis-

placed from the nominal flight path and orientation. The aircraft tracking data supports this (see figures 7, 9, and 11).

For prediction work, the assumption of symmetry leads to the conclusion that that the two sideline microphones discussed above should have the exact same measured acoustics. From this analysis, it is clear that for flight data this situation is never exactly the case, even for explicitly defined repeat flight conditions.

Acoustic Time Histories: Descent Cases

Figures 19-21 show acoustic pressure time histories for the three different descent angles and the one BVI condition. On examination of the first three descent cases, one of the most noticeable features is that, for times at and after the overhead time, the character of the acoustic pressure signals is the same for the different descent conditions. In addition, the character of these signals is essentially as that found in all of the level flight runs shown previously. As noted then, the signals appear to be thickness noise dominated. For times before the overhead time, the dominant feature in the these three descent cases is the double peak event. Some of these double peak events also have smaller pulses superimposed on them. For example, for the 6° descent case in figure 19, in the "15 sec prior" and the "10 sec prior" plots, the pulses are not smooth, but rather have other pulses included. It is speculated that these are small BVI events.

Examination of the 9° descent BVI condition, as measured from the centerline microphone, (figure 19) reveals a smooth pulse preceded by a substantial BVI event. These features are similar for all of the times prior to overhead. As expected the signals from the sideline microphones (figures 20 and 21) show double the BVI activity. For some of the times, the pulse separation times at microphone 6 and microphone 12 are substantially different. For example, in the "5 sec prior" plot for the 6° descent angle in figure 20, the pulses are almost evenly spaced. However, the corresponding plot for microphone 12 in figure 21, the pulses are very close together. For this condition there is considerable variation in the aircraft yaw, roll and pitch angles (see, figures 10, 12 and 14). The differences in distance from each rotor to microphones 6 and 12 are such as to warrant the difference in pulse separation. As with the centerline microphone data shown earlier, except for the actual BVI components of the signal, the remainder of the acoustic pressure time histories look similar to the level flight conditions.

Integrated SPL

The integrated SPL metrics, LowSPL and MidSPL, are presented as time histories from the 3 microphone locations (6, 9 and 12) and as directivity maps.

LowSPL Time Histories

Figure 22 shows time histories of the LowSPL for the centerline and sideline microphones for the four level flights. In these plots, the horizontal axis is the time relative to the overhead time. This is the same axis scale used in figures 3 through 14. The vertical axis is the LowSPL in dB and covers 70 to 120 dB. The figures here come from integrated spectra plotted at each one second interval in the 40 second interval on the horizontal axis.

In figure 22 for microphone 9, it can be seen that the LowSPL peaks about 5 seconds before the aircraft reaches the microphone array. As noted earlier, at this time the microphone array is in the plane of the rotor and the signal is dominated by thickness noise. There are relatively large variations in the LowSPL for microphone 9 before the aircraft reaches the array. This variation was also noted for the acoustic pressure time history, where a large single acoustic pulse was seen for run 1 and a smaller double peak was seen for run 3. After the aircraft passes over the array (positive times on the horizontal axis), the LowSPL decreases rapidly. Since the signal is then dominated by broadband noise (see figures 16-18). Overall, all the LowSPL time histories from all three microphones are similar. Even though the details of the time histories are comparably different in character and amplitude (one peak vs double peaks).

The LowSPL time histories for the descent conditions are shown in figure 23. The first three descent cases look very similar in character to the level flight cases. That is, the levels increase as the vehi-

cle approaches the array (time = 0), the levels peak around 5 seconds before the vehicle is overhead, and then the levels decrease rapidly after the overhead time. All three descent cases fall within about a 5 dB "band." The BVI case, on the other hand, tends to start off at a higher level and remain at that level until passing over the array. Otherwise, it should be noted that these LowSPL values for the BVI case are nearly indistinguishable from the first three descent conditions.

LowSPL Contours

LowSPL directivity is presented in figure 24. In all of these contour plots, the aircraft is located at the origin and is pointing with its nose to the right. The horizontal axis shows the fore/aft angle. The positive angles are in front of the aircraft, zero degrees points vertically downward, and the negative angles are aft of the vehicle. The vertical axis is the lateral angle. Positive angles are to starboard of the aircraft, zero degrees points vertically downward, and negative angles are to port. The actual directivity angles are as determined from the aircraft tracking data.

Examination of figure 24 reveals that the maximum noise is directed forward and down at approximately the nacelle tilt angle. This is the thickness noise effect that has been shown previously in the LowSPL time histories and shown in detail in the acoustic pressure time histories. Aft of the aircraft on either side of the centerline are low noise zones. Though there are some minor differences, these overall characteristics prevail for all of the level flight runs.

Figure 25 shows similar contour plots for the descent cases. Note that the irregular boundary shape of the figures is due to the usage of the actual directivity angles computed from the aircraft tracking data. The descent conditions, have the same overall contour map characteristic that was seen for the level flight runs, with the exception of the BVI condition. For the first three descent conditions, the maximum LowSPL occurs approximately in the plane of the rotor and minimum LowSPL occurs aft and to either side of the vehicle, as was the case for the level flight conditions. The 9° BVI descent case, with the nacelle tilt at 85° and a fuselage nose down pitch of approximately 4.5°, has a slightly different directivity pattern. The maximum LowSPL is directed such that it is nearly in the plane of the rotor.

Similarities in all of these figures are seen despite the differences seen in the acoustic pressure time histories (*i.e.*, the single pulses *vs* the double pulses *etc.*). This is due to the fact that integration tends to smooth out any differences. For prediction work, this has the implication that integrated noise metric are not necessarily the best mechanism available to examine or assess the capabilities of a prediction method to properly model specific noise sources.

MidSPL Time Histories

MidSPL time histories are shown in figures 26 and 27. (Note that the vertical axis range is now from 40 to 100 dB.) It can be seen here that there is a large variation in the levels between the four level flight runs, except in the 4 second interval around the overhead time. The explanation for this can be found in the acoustic pressure time histories near the overhead time. Those show that broadband rotor noise with similar characteristics across the set of runs dominates the acoustics in the MidSPL frequency range near the overhead time. Even so, the MidSPL component shown here is almost insignificant compared to the LowSPL values. For example, for the centerline microphone, the MidSPL peak is approximately 30 dB below the LowSPL peak. Unlike the LowSPL, which was not symmetric about the overhead position, the MidSPL plots are seen to be symmetric about this point for all three microphones.

Figure 27 shows the MidSPL time histories for the descent cases. The 3° and 9° descent conditions show similar characteristics to the level flight cases, but have an even larger variation in levels. The 6° descent case is similar to the 3° and 9° descent for the approach, but the MidSPL decreases far more rapidly than the other two cases. As for the BVI case, as before, after the array has been passed, it behaves like the 3° and 9° cases. However, on approach, there is much more MidSPL content, due to BVI, which was clearly noted in the acoustic time histories in figures 19-21.

MidSPL Contours

The MidSPL contours for the four housekeeping runs are shown in figure 28. Comparing the four housekeeping runs shows that, overall, the MidSPL footprints are similar. The contours are all roughly the same shape. They show that the MidSPL is spread over a large area from about 30° aft to about 60° forward of the aircraft and about ±60° to both sides of the vehicle. There also appear to be two maxima, near ±45°. The reason for these maxima is unknown at this time, however the levels of these maxima are very low when compared to the LowSPL in that region. Therefore, these are not dominant noise sources for these flight conditions.

Figure 29 show similar plots for the 3, 6, 9, and 9° BVI descent cases. The first two descents look very similar to the level flight cases. The 9° descent condition shows similar levels to the first two descent cases, but with a slight aft shift of the maximum MidSPL noise. The 9° BVI condition, as expected from examination of the acoustic pressure time histories, has a much higher MidSPL, which radiates forward of the vehicle.

Predictions *vs* Measurements

The examination of the measured data presented above was necessary to show the variations that are possible in the measured data, even for repeated conditions. From the aircraft state information, it was shown that the airspeed can be maintained within several knots and is relatively constant for a given run. Altitude and lateral location are maintained to within less than two rotor diameters for the level flight runs. Lateral position is also maintained less than two rotor diameters for the descent conditions, but the descent angles (altitude) can vary significantly during a intended constant descent. In fact, for the 6° and 9° descent cases, the descent angle can vary from about 3 to 10° during a run. Aircraft roll orientation is generally held to a small angle. However, yaw orientation is not necessarily maintained to a small angle and can have a first order impact on the pressure time histories due to the direct change in distance from each rotor to a given microphone. Though there is not a nominal value for the fuselage pitch angle, for the level flight cases, which are intended to be identical, it can vary between 2° and 5°. This variation would be expected to measurably alter the trim state and hence the resulting acoustics.

Comparing acoustic pressure time histories for repeated flights shows that there can be substantial variation in the character of the signal as the vehicle approaches the array. However, the character of the signal appears to be the similar for each rotor and the difference in the overall character (*i.e.*, single pulse *vs* double pulse) appears to arise from the phasing (*i.e.*, how the two signals are summed) of the signals from each rotor. In addition, all of the cases seem to produce very similar time histories at, and after, the time that the aircraft is overhead.

Noise footprints (contour plots) of LowSPL and MidSPL show that, even though substantial variations can occur in the character of the acoustic signals, the integrated quantities tend to obscure these variations.

Since it is not possible to *a priori* determine the flight conditions that will actually be flown, a prediction must start with the nominal conditions and consider flight condition variations which will cover the expected variations. This is the methodology followed in the following sections.

Flight Vehicle Trim

Given a flight condition, CAMRAD.Mod1 trims the full vehicle by balancing forces and moments on the whole vehicle. For this paper, the vehicle is trimmed in “symmetric” flight by determining the combination of governor setting, longitudinal stick setting, and the fuselage pitch angle that balances the vertical force, the longitudinal force, and the pitch moment on the whole vehicle.

During the trim iteration, for a given governor (or collective) setting, longitudinal stick setting, and fuselage pitch attitude, the rotor motion and circulation are iterated until convergence of both has occurred. Then, the pitch settings and fuselage pitch attitude are perturbed one at a time and the rotor motion and circulation are converged again for each perturbation. This technique produces a “derivative matrix” that is used to compute successive values of the settings and fuselage pitch attitude for the trim iterations. The trim iteration is considered con-

verged when a particular normalized combination of the forces and moments falls below a specified tolerance [18].

For this paper, aerodynamic forces and moments generated by the fuselage are computed using a single look-up table that lumps the aerodynamics of the wing, the body, and the tail into one table [20]. The table does not include any rotor/fuselage interaction effects. This table uses fuselage angle of attack, side slip angle, nacelle tilt angle, and deflections of the aileron, flap, elevator, and rudder as independent parameters. The rotor dynamics are generated using the internal CAMRAD.Mod1 blade dynamics model, given the blade properties. The rotor blade aerodynamics for trim are computed at every spanwise and radial collocation position on the blade, with the use of airfoil tables and the internal CAMRAD.Mod1 blade aerodynamics model. A model for yawed and swept flow is included in the blade aerodynamics model, but the effect of sweep on blade dynamics is not included.

Rahnke[20] compared the measured trim fuselage angle of attack to three different fuselage aerodynamics models. One of the models, labeled "CAMRAD 99" in Figure 7 of [20], involves the same fuselage aerodynamic table used here. Using the current model, a comparison of predicted fuselage angle of attack (which is the same as the fuselage pitch attitude for a level flight condition) for the speed range shown in Figure 7 of Rahnke [20] shows good agreement with both the "GTR" model and the "CAMRAD 99" models. Since there is no measured data in the speed range of interest here (90 to 98 knots), linear extrapolation of the measured data from lower speeds shows the current model results are near the extrapolated measured data. In addition to these prediction comparisons, examination of the range of measured airspeeds and the range of measured fuselage angles of attack in figures 3 through 14 show that they compare well to Figure 7 of Rahnke, especially since Rahnke states an uncertainty in the measured data of up several degrees. Comparisons of measured and predicted rotor shaft horsepower (also shown in Rahnke's Figure 7) show that, in the speed range of interest here, our predictions match well with the "CAMRAD 97" and the "GTR" models. However, all of these models under-predict the measured power slightly.

Descent Angle[γ°]	Fuselage pitch[$^\circ$]	Rotor AOA[$^\circ$]	Rotor Lift Fraction
0°	5.0	24.0	0.456
3°	3.9	22.1	0.408
6°	2.9	20.0	0.355
9°	2.3	17.3	0.316
9° BVI	-3.3	0.7	0.673

Table 2: Predicted trim values using the nominal flight condition as input to TRAC.

Vehicle Trim: Nominal Conditions

The predicted aircraft trim state using the nominal flight conditions from Table 1 is shown in Table 2. The vehicle nominal weight for these conditions is 13,200 pounds, however, during the test, the weight could vary as much as 10% based on fuel burn. The fuselage pitch angle is positive nose up; the rotor angle of attack is positive nose down; and the rotor lift fraction is defined as the ratio of the total rotor lift (from both rotors) to the total vehicle weight (the remaining lift fraction is carried by the wings, fuselage, *etc.*).

From the first four entries in Table 2 it can be seen that as the descent angle increases, the fuselage pitch angle decreases, the rotor angle of attack decreases, and the fraction of aircraft weight that is carried by the rotors decreases. That is, in level flight, the fuselage is generating about one half of the lift, but in a relatively steep descent of 9° at the same airspeed and nacelle tilt, the fuselage is generating nearly 70 percent of the lift for the vehicle. For the BVI condition, the rotor is at a nacelle tilt of 85°, the airspeed is approximately 70 knots. The fuselage pitch angle trims to about -3.3°, the rotor angle of attack is less that 1°, and the rotors are carrying over 2/3 of the vehicle weight.

In a free flight trim, there are few parameters that are "adjustable" in a meaningful way which will affect the trim. One such "adjustable" parameter that is different between the nominal conditions and the actual conditions is the airspeed. The airspeed will affect both the trim of the vehicle and hence the resulting acoustics. Since CAMRAD.Mod1 does not have the capability to execute a non-steady flight trim, only two prediction techniques are examined

here. The first technique, labeled "Prediction One," is a standard technique which would be used in a true prediction. Prediction One is executed using only the nominal flight conditions for the aircraft. This nominal condition is used in both the CAMRAD.Mod1 computation and the WOPMOD acoustic prediction. The second technique, labeled "Prediction Two," is designed to examine the effect of aircraft position and orientation on the prediction. Since CAMRAD.Mod1 uses only a steady state trim, the results of Prediction One are used in the Prediction Two technique. The Prediction Two acoustics are computed using the optically measured aircraft position (at the retarded time for a given microphone and time) and the onboard measured orientation of the vehicle (again, at the retarded time). These measured quantities are input to the acoustic analysis, WOPMOD as a function of time in a quasi-steady manner.

Acoustic Time Histories: Prediction One

The predicted acoustic pressure time histories for the level flight and non-BVI descent cases are shown in figures 30 through 33. These are presented in a slightly different format from the measured data. Since these are for nominal conditions, each flight condition is shown as a separate figure. The three rows in each figure are for the centerline microphone ("mic 9") and the two sideline microphones used previously ("mic 6" and "mic 12"). It can be seen that in all of these cases, for the centerline microphone, there is only a single pulse. This is because the signals from each rotor arrive at the centerline microphone at exactly the same time, due to the symmetry of the nominal condition. Likewise, the signals from the two sideline microphones are identical also due to the symmetry condition. The sideline microphone signals, as expected, contain the double pulses.

Overall all the time histories for the level flight and glideslope sweep exhibit the same general character. There are impulsive features, but not BVI as the aircraft approaches the array. This is consistent with what was observed in the measured data. As the aircraft is overhead, the signal changes to low frequency loading noise, which continues as the aircraft passes the array. Note that there is no broadband component included in the prediction.

For the BVI condition in figure 34, there is evidence of BVI events. However, they are dominant primarily in the "5 sec after" overhead plot. The measured data for this case (figure 19) contain BVI for all times shown. At times before the aircraft was overhead the measured data contain very strong, prominent BVI events and less significant BVI events after the aircraft is overhead. Much success has been reported in comparing predicted with measured BVI tiltrotor noise obtained from wind tunnel tests [11, 12, 14]. In those tests, the rotor conditions (*i.e.*, rotor thrust, rotor angle of attack, rotor moments, and advance ratio) were all known and measured. For the flight test, none of these are known or measured to any degree of accuracy, except the advance ratio. Predicted BVI noise is known to be sensitive to, and a direct function of, the rotor thrust, rotor angle of attack, and advance ratio.

Flight predictions using TRAC determine the rotor thrust, rotor angle of attack, and rotor collective (governor) and longitudinal cyclic settings based on summing the forces and moments for the entire aircraft. As explained earlier, the aircraft fuselage (wing, body, and tail) aerodynamics are lumped into one table. The effect of rotor downwash and any other rotor/fuselage interactional effects are not accounted for in this table. The determination of the lift share between the rotor and the fuselage will be in error, particularly for low speed flight. The magnitude of the error is not known at this time. However, based on the estimates used for planning two tiltrotor wind tunnel tests (references [12] and [14]), the predicted rotor thrust for this BVI flight condition is about 20% low. TRAC predictions for an isolated XV-15 rotor with the higher rotor thrust produce significant BVI events. The main difference between these and the predictions made for flight is the unknown lift share between the body and the rotors, which is, to first order, a direct function of the body table and overall trim procedure within CAMRAD.Mod1. In order to significantly advance tiltrotor flight prediction methods, particularly for BVI flight conditions, accurate measurements of the rotor state, (*i.e.*, rotor thrust, rotor tip-path-plane angle, and aircraft body orientation) must be made

available.

LowSPL: Prediction One

Figure 35 shows the integrated LowSPL time history for the level flight condition, along with the range of measured data. (The measured data band is the minimum and maximum LowSPL values at each time on the horizontal axis.) It can be seen that the overall features are the same as the measured data shown in figure 22. That is, the level increases as the aircraft approaches the array, the level peaks approximately 2 seconds before the aircraft reaches the array, and the level decreases dramatically after the aircraft passes the array. The decrease in predicted levels after the aircraft has passed the array is larger than the measured decrease. The location of the peak level is well predicted, but the peak level itself is underpredicted. The measured data also showed that the peak level for the sideline microphones is lower than for the centerline microphone; this same trend is seen in the prediction.

Figure 36 shows the descent cases, including the BVI case. The corresponding measure data can be seen in figure 23. Also on figure 36 is the range of measured data for all of the descent cases. The non-BVI cases show the same trends as the level flight cases and compare in a similar fashion to the measured data. However, the BVI condition does not follow the same trend as the measured data shown in figure 23, but it does fall with in the measured band of data for the descent cases.

Figure 37 is the LowSPL contour plot for the level flight case for Prediction One. Again, note that there is only one figure since this prediction is for the nominal flight condition, which is identical for all four of the level flight cases. The predicted LowSPL directivity has the same general features as the measured directivities shown in figure 24. That is, the maximum LowSPL is in front of the vehicle, primarily in the plane of the rotor (*i.e.*, 60° on the horizontal axis). The minimum LowSPL noise is aft of the vehicle, with two "lobes" centered at approximately $\pm 45^\circ$. The Prediction One LowSPL contours for the descent cases are shown in figure 38. Again, the contours of the first three descent cases have the same general characteristic shape as the measured data (figure 25). As the descent angle becomes steeper, the maximum LowSPL shifts slightly forward and the two minima aft of the vehicle become more focussed and are moved slightly outboard. The predicted BVI case contours also follow the same trend as the measured data. That is, the maximum LowSPL is spread over a larger area, extending from directly beneath to far forward of the vehicle. Also, both the measured and predicted data show that the minimum "lobes" are no longer present.

Since the primary component of the MidSPL for these cases is broadband noise, and since there is currently no broadband included in the predictions, no predicted results are shown here for the MidSPL.

Acoustic Time Histories: Prediction Two

Figures 39 through 44 are the predicted acoustic pressure time histories for the level flight and descent cases. These "Prediction Two" cases use the exact same loading information from CAMRAD.Mod1 as in the "Prediction One" cases. However, in the noise computation (WOPMOD), instead of using observer locations computed from the nominal position and orientation of the vehicle and assuming symmetry, the observer locations are computed for each rotor using the optically measured position (longitudinal, lateral, and altitude) and onboard measured orientation (yaw, pitch and roll attitude). As can be seen from these predictions, the small changes in vehicle orientation can have a substantial impact on the acoustic pressure time histories. This can be dramatically seen in several figures.

Figure 39 shows the centerline microphone for the four repeated level flight cases. All the results contain two distinct pulses. In the Prediction One results, this centerline microphone always has a single pulse because the rotors are symmetrically placed about the microphone. Figure 40 and 41 show the predictions for the sideline microphones. Two of the cases have a single pulse for microphone 6 while microphone 12 always has two distinct pulses with a variable time between pulses for each run. Prediction One results for the sideline microphones always show two pulses because the rotors are symmetric about the microphone. For all of these non-nominal conditions, the problem is now

asymmetric. The sensitivity of the acoustic pressure time histories to the actual orientation of the vehicle, even when position and orientation perturbations are relatively small, was speculated to be the root cause of the anomalies seen in the measured time histories presented earlier. Comparing the Prediction One results to the Predictions Two results, this sensitivity is clearly seen to be a factor. Though there are no repeated descent conditions to compare with, this trend is seen to hold in the descent cases as well in figures 42 through 44.

Though these predictions account for measured position and orientation of the vehicle, the measured blade position has not been included since it was not measured. The predictions show that the acoustic pressure time histories are very sensitive to position and orientation. Even the measured data showed that the small differences in distance between sources have a large impact on the acoustic time histories. Since even the azimuthal location of the blades as a function of time is not known, large differences in blade position are possible between the measured and predicted acoustics. Based on the double pulses, even distance differences on the order of a couple of feet can result in drastically different acoustic time histories. Differences even as small as those created by the unknown azimuthal location of the blades can possibly account for many of the differences seen in the measured and predicted acoustic pressure time histories.

LowSPL: Prediction Two

Figure 45 shows the integrated LowSPL time history for the level flight condition for Prediction Two along with the range of measured data from figure 22. It can be seen that the overall features are the same as the measured data and as the Prediction One data shown in figure 35. Here, less than 3 dB difference can be seen for microphone 9 and 12 for these integrated quantities. These differences are caused by the position and orientation differences between the runs. However, as much as 5-6 dB difference between the runs can be seen for microphone 6. Also, significant differences can be seen between the two sideline microphones. Compared to the measured data range, these predictions are better than those in Prediction One. Figure 46 shows the integrated LowSPL time history for the descent conditions for Prediction Two. For the non-BVI descents, variations similar to those seen in the measured data are shown in the predictions. And, as with the level flight cases, there are significant differences between the two sideline microphones. The BVI descent condition underpredicts the LowSPL before the vehicle passes over the array, but does well after the aircraft passes the array. It is speculated that the general underprediction of the low frequency noise component is due to low frequency rotor loading predictions. This low frequency rotor loading is directly related to the vehicle trim conditions and lift share between the aircraft fuselage and the rotors. However, there were no measurements made of the rotor loading.

Figures 47 and 48 show the difference in LowSPL between the two prediction methods. These are the Prediction One results subtracted from the Prediction Two results. These show that there is a significant difference in the predictions when the actual aircraft position and orientation are included. For the level flight cases, as much as 6 dB difference is seen when these effects are included. For the descent cases, the predictions can show nearly a 10 dB difference when the position and orientation are taken into account.

Figure 49 shows the LowSPL contour plots for the Prediction Two level flight cases. The predicted levels are very similar to the Prediction One case, but the contours are now asymmetric about the aircraft plane of symmetry. Since the loading information is the same as in the Prediction One case, this asymmetry is due to the differences in position and orientation of the vehicle. It should be noted that, even though the predicted acoustic pressure time histories showed many differences in character between the four level flight runs (due to the location and orientation differences), these contour plots are all very similar in character.

As with the Prediction One case, since the main contribution to the MidSPL is broadband (except for the BVI condition), and since no broadband information is used in the predictions, so no MidSPL predictions are shown here.

Conclusions

A subset of data from a 1995 XV-15 flight test has been examined in detail. The actual flight conditions and state of the aircraft were examined and compared to the nominal conditions for four repeated level flights and for four descent conditions. Acoustic pressure time histories were examined for a centerline microphone and two symmetrically placed sideline microphones. For the repeated level flight cases, differences in these time histories show that the time histories are very sensitive to changes in flight conditions. While the variations in the flight conditions can be considered small in terms of vehicle performance, they have a large impact on the acoustic pressure time histories. Examination of contours LowSPL and MidSPL revealed that, even though there were substantial differences in the character of the acoustic pressure time histories, the integrated quantities show little difference between the cases, as expected.

Examination of measured data from the descent conditions showed that there can be substantial variation in the descent angles for a nominally constant descent. Since the variation in the descent angles is on the order as the differences in the intended nominal conditions, and since the conditions were not repeated, interpretation of results is difficult. The LowSPL and MidSPL for the descent cases showed the same general characteristics between the cases.

TRAC has been used to predict tone noise components using two techniques. The first technique, which uses only the nominal conditions, showed that using the symmetry condition for the acoustic predictions can be misleading when comparing to measured acoustic pressure time histories. This is due to the sensitivity of the measured data to the vehicle position and orientation discussed above. The second technique, which includes effects of vehicle and orientation, shows the effect of these quantities on the acoustic pressure time histories. Though differences between the cases are shown in the predictions, other unknown quantities limit the accuracy of the predictions. Two such quantities are the rotor thrust (lift share) and the rotor angle of attack. In a wind tunnel test, the rotor thrust and angle of attack are known accurately and prediction methods can match those conditions well. For a free flight test however, the rotor thrust and angle of attack are normally not measured and the prediction method must determine the rotor thrust and angle of attack as part of a global vehicle trim scheme. As such, there is no way to know if the rotor conditions are matched between the flight and prediction. Since BVI noise is very sensitive to the rotor thrust and angle of attack, some measure of these quantities must be made available in order to systematically improve predictions in the future.

In addition to the above, the predictions also do not address unsteady flight effects, which can have a substantial effect on the blade loading and acoustics. The low frequency loading is related to the low frequency noise characteristics of the vehicle. However, the rotor loading was not measured in this flight test. Again, these quantities need to be available in the future as a diagnostic tool to improve predictions.

Though the measured time histories showed substantial differences in character, the integrated quantities (*i.e.*, LowSPL) show only small variations between the difference cases. As such these integrated quantities alone are not an adequate measure of the success of a prediction method. Also, as with the measured data, it was shown that the Prediction One results and Prediction Two results show small differences between the cases. However, it was shown that the actual vehicle position and orientation can have a significantly impact on the predicted acoustics.

Acknowledgments

The authors would like to recognize the assistance of Mr. Charles Smith of Lockheed Martin for providing raw measured data, Mr. Dave Conner of the Army and Mr. Bryan Edwards of Bell Helicopter Textron for providing guidance on the actual test and aircraft conditions, Dr. Wayne Johnson and Mr. W. C. Acree, Jr. of Ames Research Center for providing aircraft property data, Dr. Devon Prichard of Virginia Polytechnic Institute of Technology (formerly of Lockheed Martin) for his work on TRAC, and Dr. Tom Brooks and Dr. Feri Farassat of NASA Langley Research Center for their many helpful discussions and guidance on this subject.

References

[1] Marcolini, M.A., Burley, C.L., Conner, D.A., Acree, Jr., C.W., "Overview of Noise Reduction Technology of the NASA Short Haul (Civil Tiltrotor) Program," SAE Paper 962273, International Powered Lift Conference, Jupiter, FL, November 8-10, 1996.

[2] Edwards, B.D., "XV-15 Tiltrotor Aircraft Noise Characteristics," 46th AHS Annual Forum, Fort Worth, TX, May 9-11, 1990.

[3] Conner, D.A. and Wellman, J.B., "Hover Acoustic Characteristics of the XV-15 with Advanced Technology Blades," AIAA Journal of Aircraft, Vol. 31, No. 4, 1994.

[4] Conner, D.A., Marcolini, M.A., Edwards, B.D., Brieger, J.T., "XV-15 Tiltrotor Low Noise Terminal Area Operations," 53rd AHS Annual Forum, Virginia Beach, VA, April-May 1997.

[5] Edwards, B.D., "XV-15 Low-Noise Terminal Area Operations Testing," NASA CR-1998-206946, February 1998.

[6] Hoad, D.R., Conner, D.A., Rutledge, C.K., "Acoustic Flight Test Experience With the XV-15 Tiltrotor Aircraft With the Advanced Technology Blade (ATB)," 14th DGLR/AIAA Aeroacoustics Conference, Aachen, Germany, May 1992.

[7] Marcolini, M.A., Conner, D.A., Brieger, J.T., Becker, L.E., Smith, C.D., "Noise Characteristics of a Model Tiltrotor," 51st AHS Annual Forum, Fort Worth, TX, May 1995.

[8] Liu, S.R., Brieger, J., Peryea, M., "Model Tiltrotor Flow Field/Turbulence Ingestion Noise Experiment and Prediction," 54th AHS Annual Forum, Washington, D.C, May 1998.

[9] Polak, D.R. and George, A.R., "Flowfield and Acoustic Measurements From a Model Tiltrotor in Hover," AIAA Journal of Aircraft, Vol. 35, No. 6, December 1998.

[10] Prichard, D.S., Boyd, Jr., D.D., Burley C.L., "NASA/Langley's CFD-Based BVI Rotor Noise Prediction System: (ROTONET/FPRBVI) An Introduction and User's Guide," NASA TM 109147, November 1994.

[11] Brooks, T.F., Boyd, Jr., D.D., Burley, C.L., Jolly, Jr., R.J., "Aeroacoustic Codes for Rotor Harmonic and BVI Noise-CAMRAD.Mod1/HIRES," AIAA Paper No. 96-1735, 1996.

[12] Burley, C.L., Marcolini, M.A., Brooks, T.F., Brand, A.G., Conner, D.A., "Tiltrotor Aeroacoustic Code (TRAC) Predictions and Comparison with Measurements," 52nd AHS Annual Forum, Washington, D.C., June 4-6, 1996.

[13] Boyd, Jr., D.D., Brooks, T.F., Burley, C.L., Jolly, Jr., J.R., "Aeroacoustic Codes for Rotor Harmonic and BVI Noise-CAMRAD.Mod1/HIRES: Methodology and User's Manual," NASA TM 110297, March 1998.

[14] Burley, C.L., Brooks, T.F., Marcolini, M.A., "Tiltrotor Aeroacoustic Code (TRAC) Prediction Assessment and Initial Comparison with TRAM Test Data," 25th European Rotorcraft Forum, Rome, Italy, September 1999.

[15] Prichard, D.S., "Initial Tiltrotor Aeroacoustic Code (TRAC) Predictions for the XV-15 Flight Vehicle and Comparison with Flight Measurements," 56th AHS Annual Forum, Virginia Beach, VA, May 2-4, 2000.

[16] JanakiRam, R.D., Khan, H., "Prediction and Validation of Helicopter Descent Flyover Noise," 56th AHS Annual Forum, Virginia Beach, VA, May 2-4, 2000.

[17] Brooks, T.F., Boyd, Jr., D.D., Burley, C.L., Jolly, Jr., R.J., "Aeroacoustic Codes for Rotor Harmonic and BVI Noise-CAMRAD.Mod1/HIRES," Journal of the American Helicopter Society, April 2000.

[18] Johnson, W., "A Comprehensive Analytical Model of Rotorcraft Aerodynamics and Dy-

namics, Part I: Analysis Development," NASA TM 81182, June 1980.

[19] Johnson, W., "A Comprehensive Analytical Model of Rotorcraft Aerodynamics and Dynamics, Part II: User's Manual," NASA TM 81183, July 1980.

[20] Rahnke, C., "XV-15 Aerodynamic Model and Blade Tip Acoustic Study," Bell Report No. 699-099-507, August 12, 1999.

[21] Beddoes, T.S., "A Near Wake Dynamic Model," Proceedings of the AHS Specialists Meeting on Aerodynamics and Aeroacoustics, February 1987.

[22] Beddoes, T.S., "Two and Three Dimensional Indicial Methods for Rotor Dynamic Airloads," AHS National Specialists Meeting on Rotorcraft Dynamics, November 1989.

[23] Beddoes, T.S., Leishman, J.G., "A Generalised Model for Airfoil Unsteady Aerodynamics Using the Indicial Method," 42nd AHS Annual Forum, June 1986.

[24] Beddoes, T.S., Leishman, J.G., "A Semi-Empirical Model for Dynamic Stall," Journal of the American Helicopter Society, July 1989.

[25] Brentner, K.S., "Prediction of Helicopter Rotor Discrete Frequency Noise," NASA TM 87721, October 1986.

[26] Brooks, T.F., Jolly, Jr., R.J., Marcolini, M.A., "Helicopter Main-Rotor Noise: Determination of Source Contributions Using Scaled Model Data," NASA TP 2825, August 1988.

[27] Burley, C.L., Brooks, T.F., Splettstoesser, W.R., Schultz, K.-J., Kube, R., Bucholtz, H., Wagner, W., Weitemeyer, W., "Blade Wake Interaction Noise for a BO-105 Model Main Rotor," AHS Technical Specialists' Meeting For Rotorcraft Acoustics and Aerodynamics, Williamsburg, VA, October, 28-30, 1997.

[28] "Tilt Rotor Research Aircraft Familiarization Document," NASA TMX-62407, January 1975.

[29] Hardin, J.C., "Introduction to Time Series Analysis," NASA Reference Publication 1145, Second Printing, November 1990.

[30] Bendat, J.S., Piersol, A.G., "Engineering Applications of Correlation and Spectral Analysis," pp. 75-76, A Wiley-Interscience Publication, John Wiley & Sons, Inc., ISBN 0-471-05887-4, 1980.

[31] Brieger, J.T., Maisel, M.D., Gerdes, R., "External Noise Evaluation of the XV-15 Tiltrotor Aircraft," AHS National Specialists' Meeting on Aerodynamic and Aeroacoustics, Arlington, TX, February 25-27, 1987.

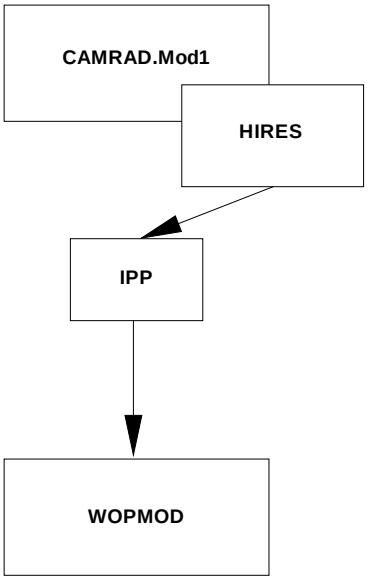

Figure 1: Schematic of TRAC used in this paper.

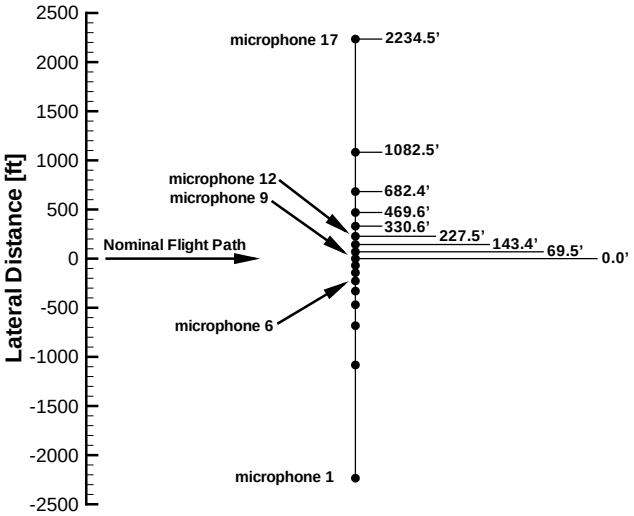

Figure 2: Microphone layout for Phase I part of 1995 flight test.

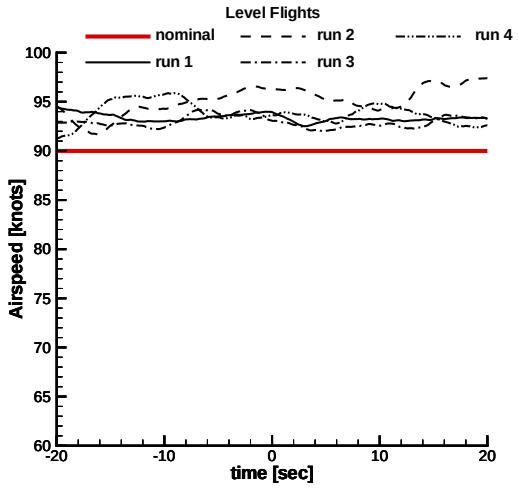

Figure 3: Measured airspeed for level flight runs 1 through 4 (the aircraft is overhead at t= 0).

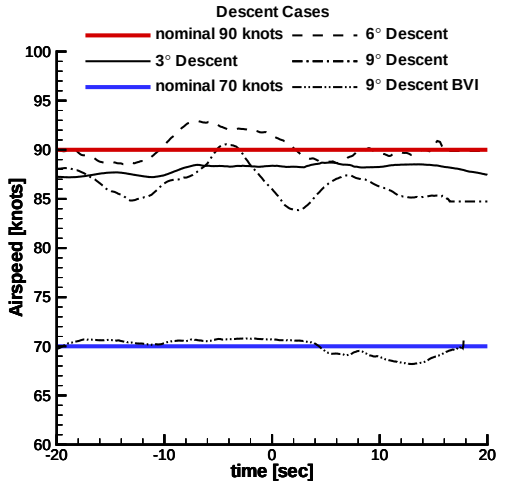

Figure 4: Measured airspeed for descent flight conditions (the aircraft is overhead at t= 0).

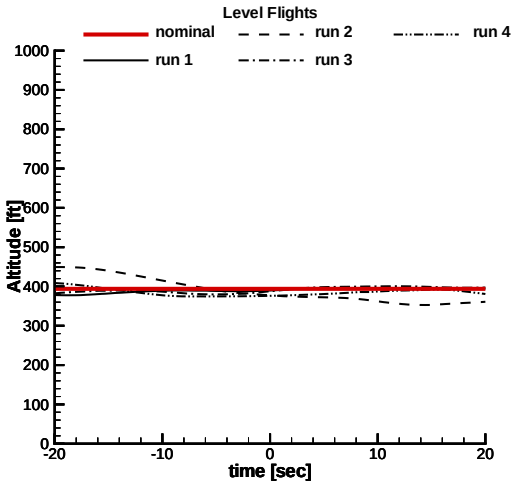

Figure 5: Measured altitude for level flight runs 1 through 4 (the aircraft is overhead at t= 0).

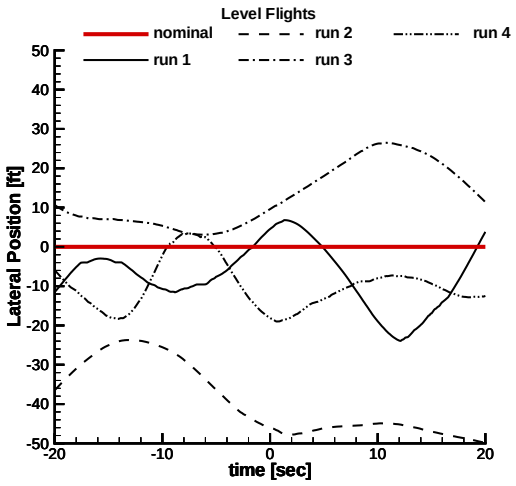

Figure 7: Measured lateral position for level flight runs 1 through 4 (the aircraft is overhead at t= 0).

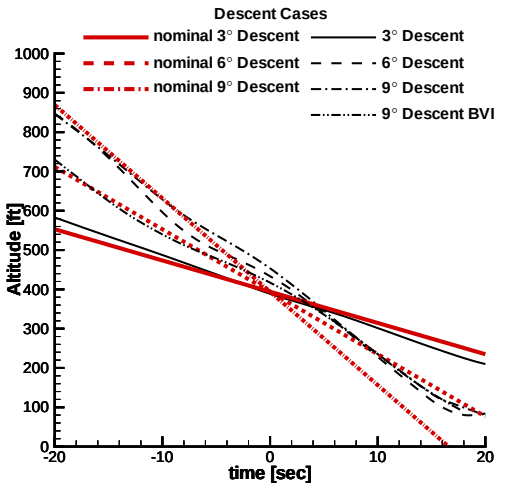

Figure 6: Measured altitude for descent flight conditions (the aircraft is overhead at t= 0).

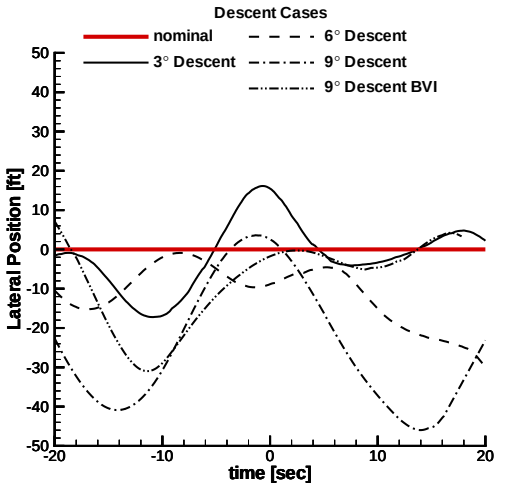

Figure 8: Measured lateral position for descent flight conditions (the aircraft is overhead at t= 0).

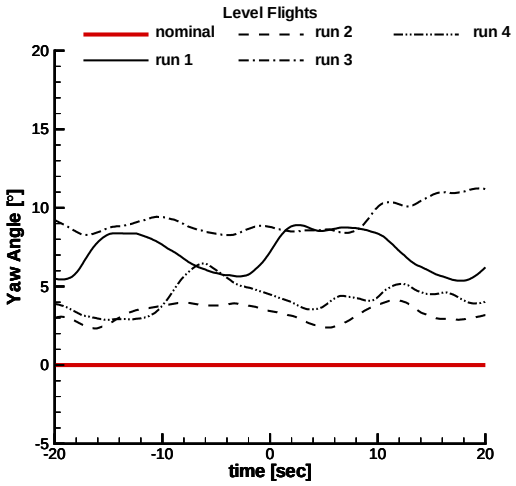

Figure 9: Measured yaw angle for level flight runs 1 through 4 (the aircraft is overhead at t= 0).

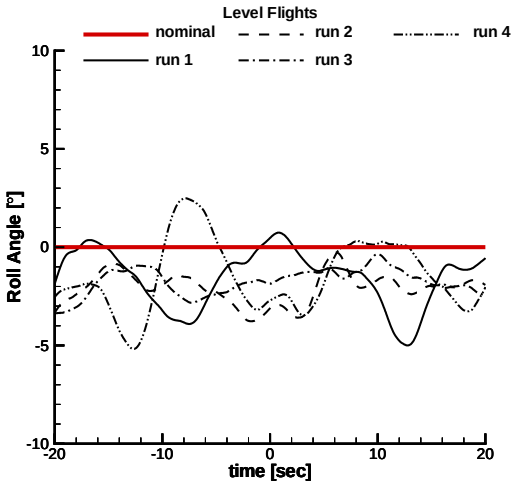

Figure 11: Measured roll angle for level flight runs 1 through 4 (the aircraft is overhead at t= 0).

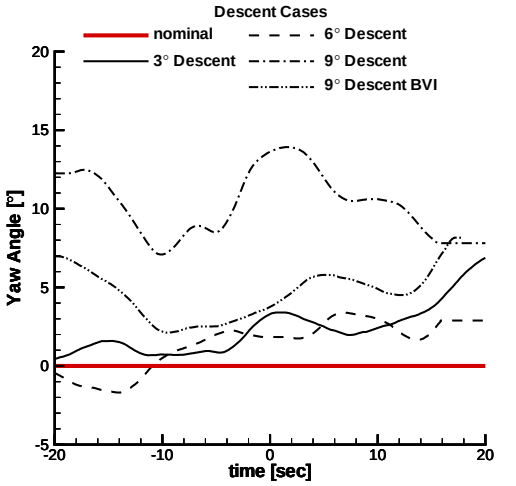

Figure 10: Measured yaw angle for descent flight conditions (the aircraft is overhead at t= 0).

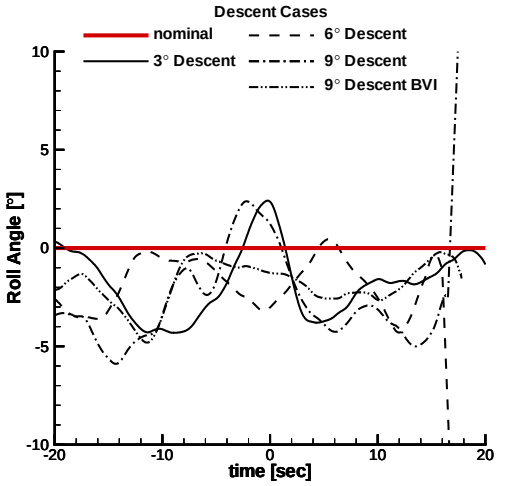

Figure 12: Measured roll angle for descent flight conditions (the aircraft is overhead at t= 0).

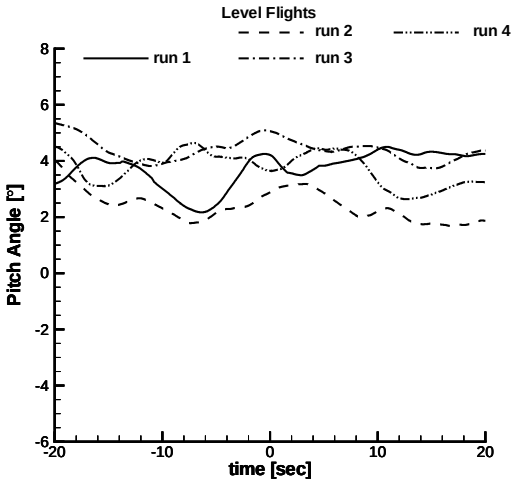

Figure 13: Measured pitch angle for level flight runs 1 through 4 (the aircraft is overhead at t= 0).

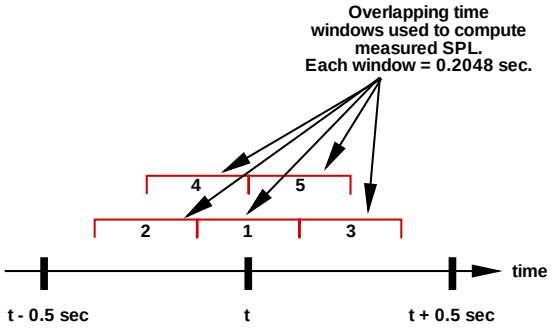

Figure 15: Schematic of time windows used to compute SPL from measured data.

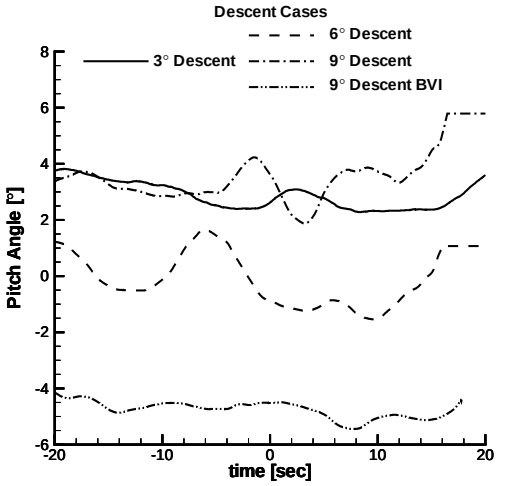

Figure 14: Measured pitch angle for descent flight conditions (the aircraft is overhead at t= 0).

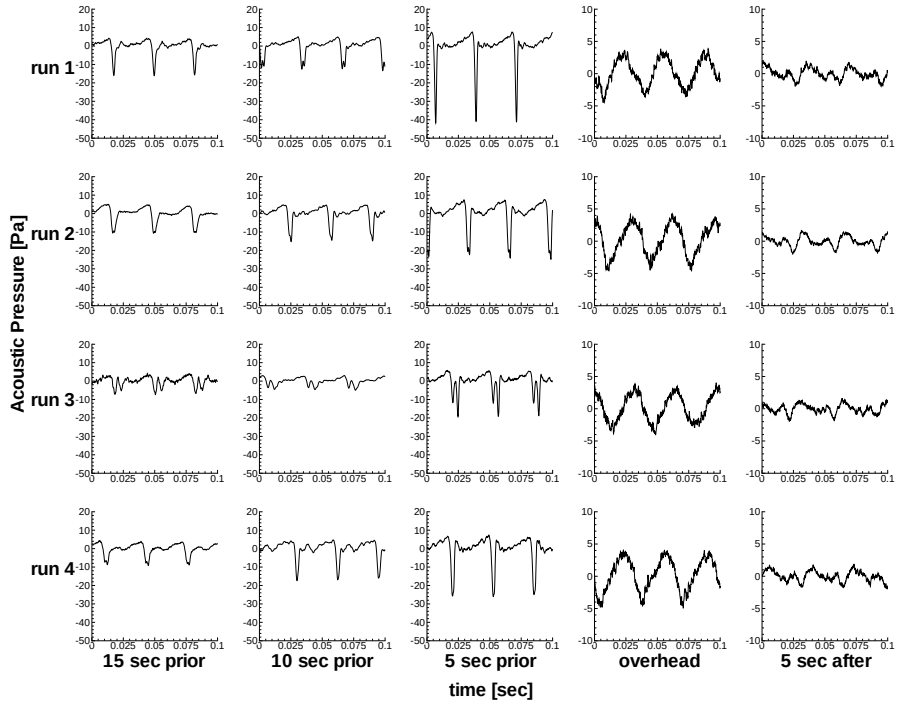

Figure 16: Acoustic pressure time histories (normalized) for the centerline microphone 9 for level flight conditions, time is relative to the aircraft overhead of the microphone array.

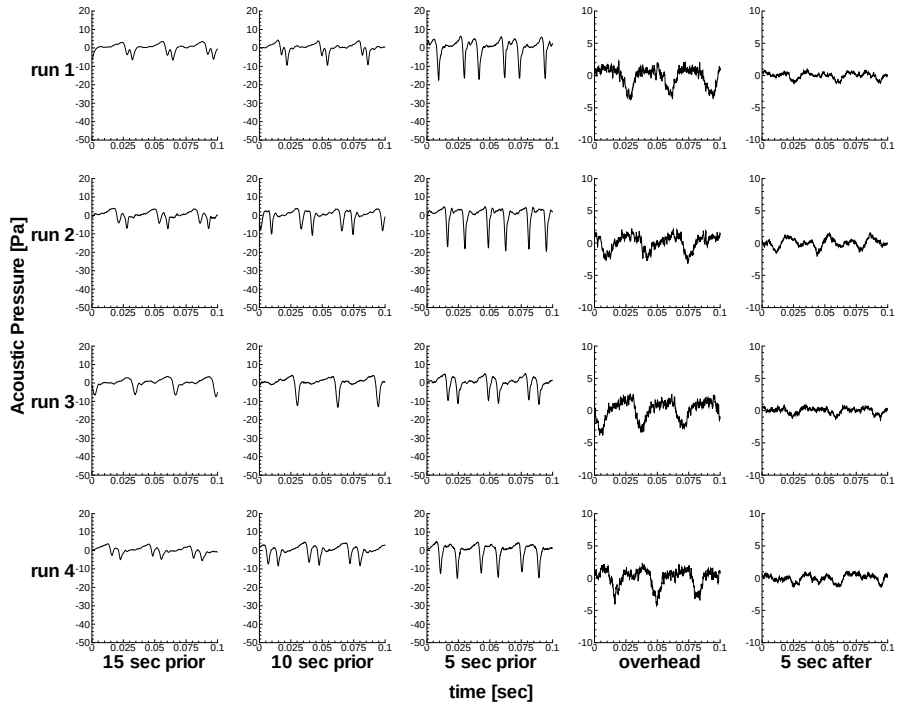

Figure 17: Acoustic pressure time histories (normalized) for the starboard sideline microphone 6 for level flight conditions, time is relative to the aircraft overhead of the microphone array.

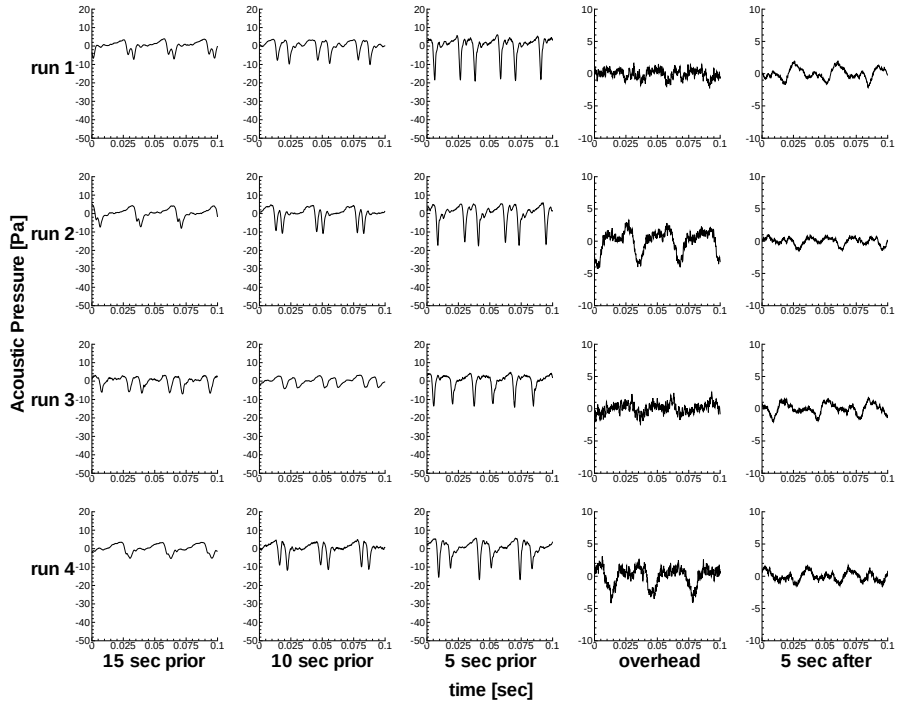

Figure 18: Acoustic pressure time histories (normalized) for the port sideline microphone 12 for level flight conditions, time is relative to the aircraft overhead of the microphone array.

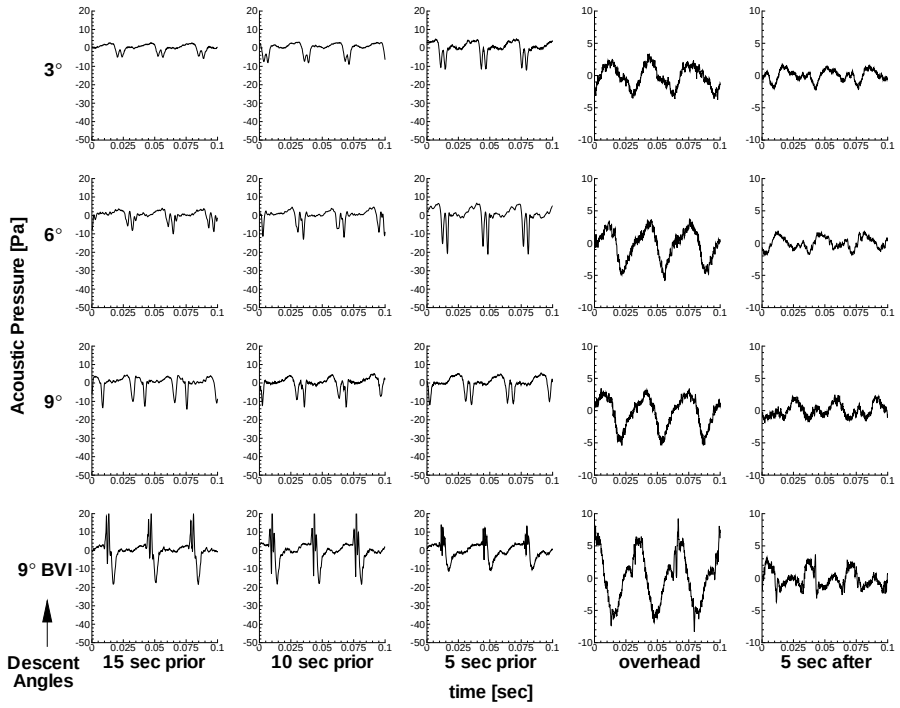

Figure 19: Acoustic pressure time histories (normalized) for the centerline microphone 9 for descent flight conditions, time is relative to the aircraft overhead of the microphone array.

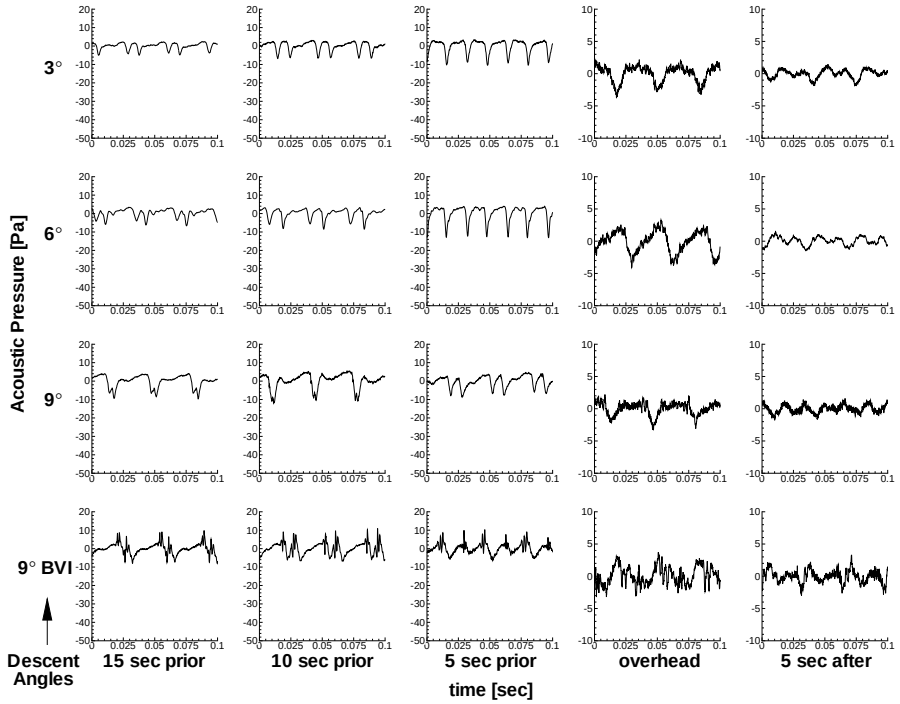

Figure 20: Acoustic pressure time histories (normalized) for the starboard sideline microphone 6 for descent flight conditions, time is relative to the aircraft overhead of the microphone array.

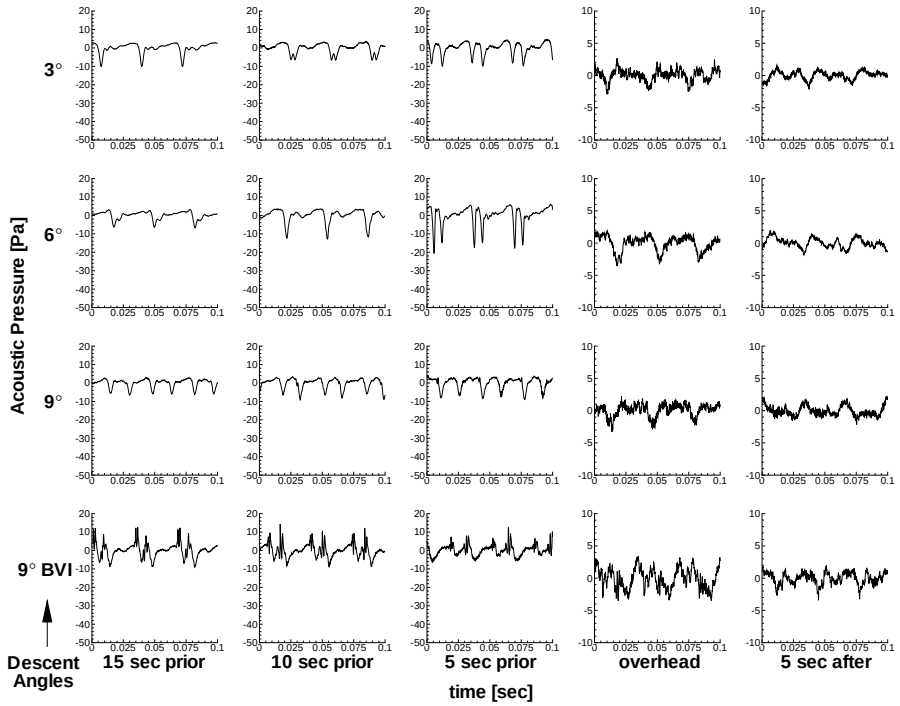

Figure 21: Acoustic pressure time histories (normalized) for the port sideline microphone 12 for descent flight conditions, time is relative to the aircraft overhead of the microphone array.

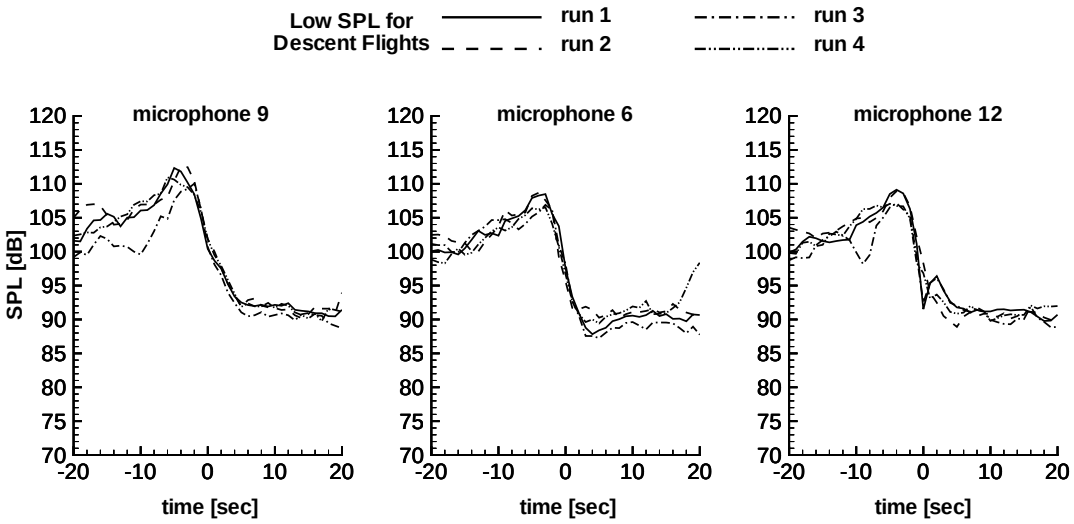

Figure 22: LowSPL time histories for level flights (the aircraft is overhead at t= 0).

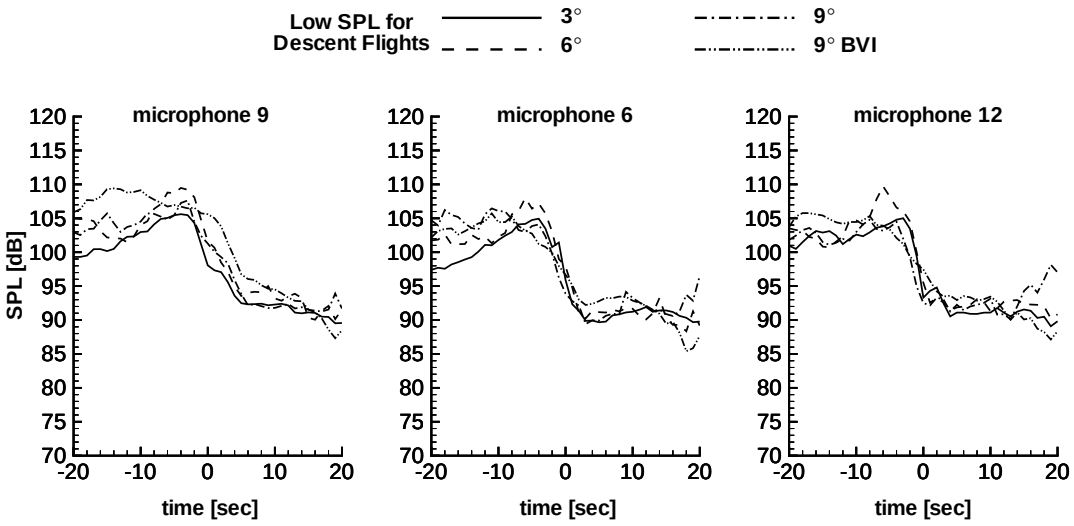

Figure 23: LowSPL time histories for descent flights (the aircraft is overhead at t= 0).

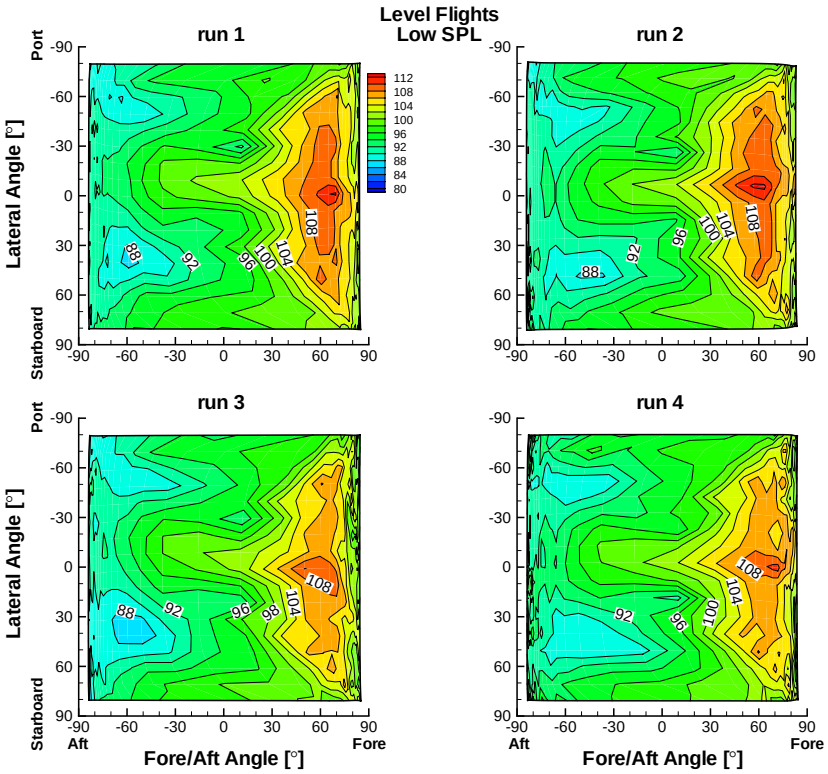

Figure 24: LowSPL contours for level flights.

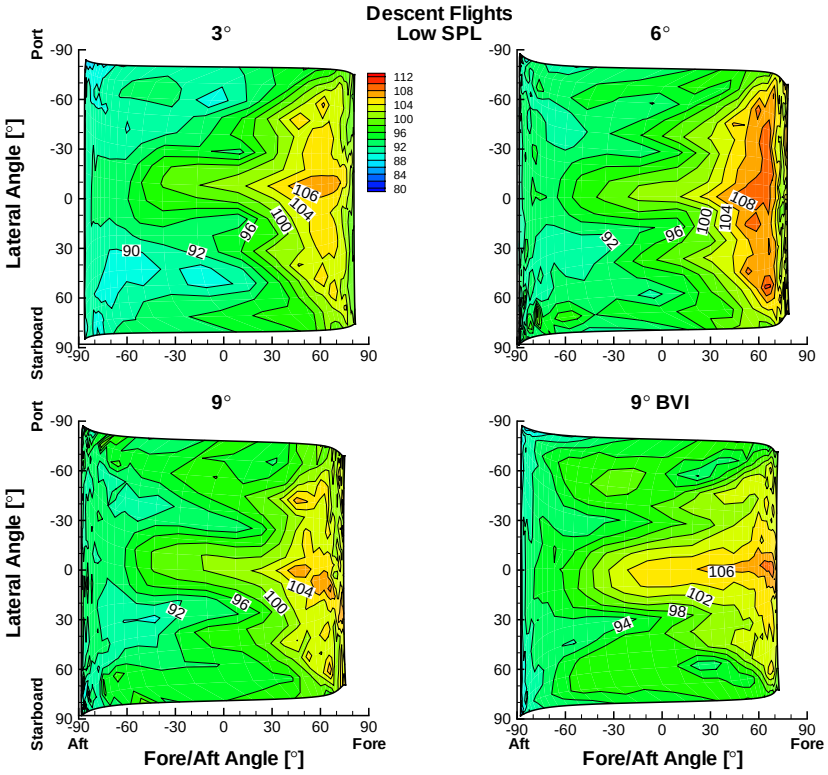

Figure 25: LowSPL contours for descent flights.

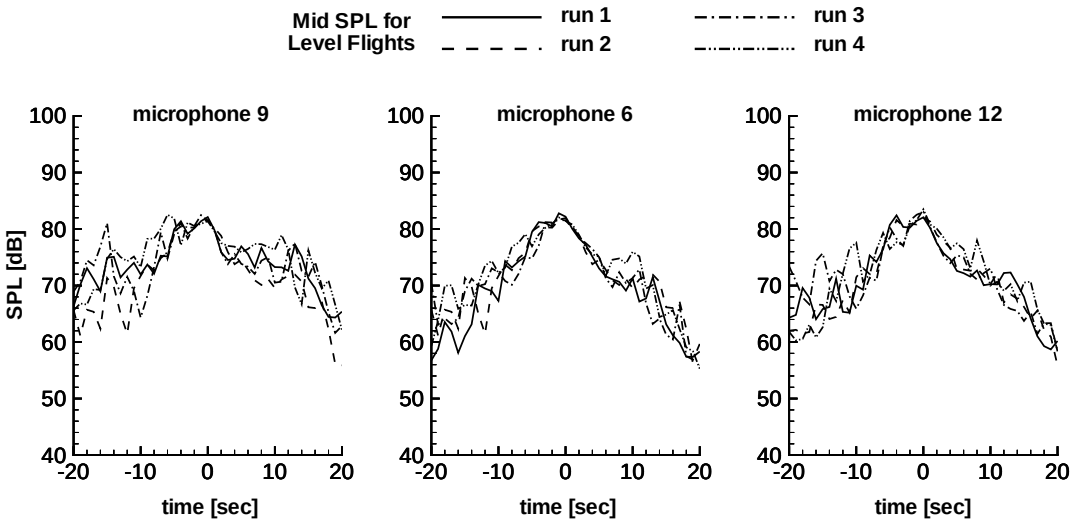

Figure 26: MidSPL time histories for level flights (the aircraft is overhead at t= 0).

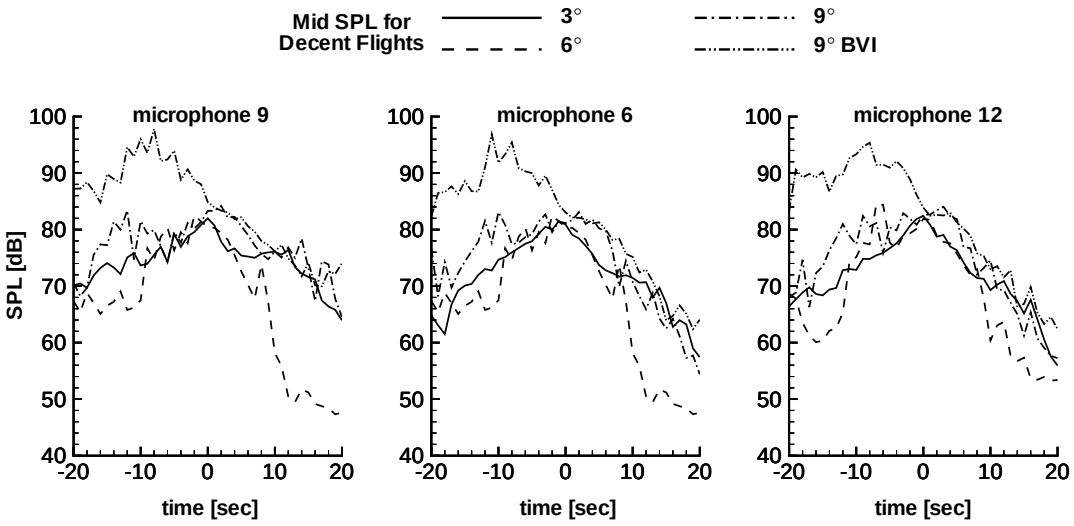

Figure 27: MidSPL time histories for descent flights (the aircraft is overhead at t= 0).

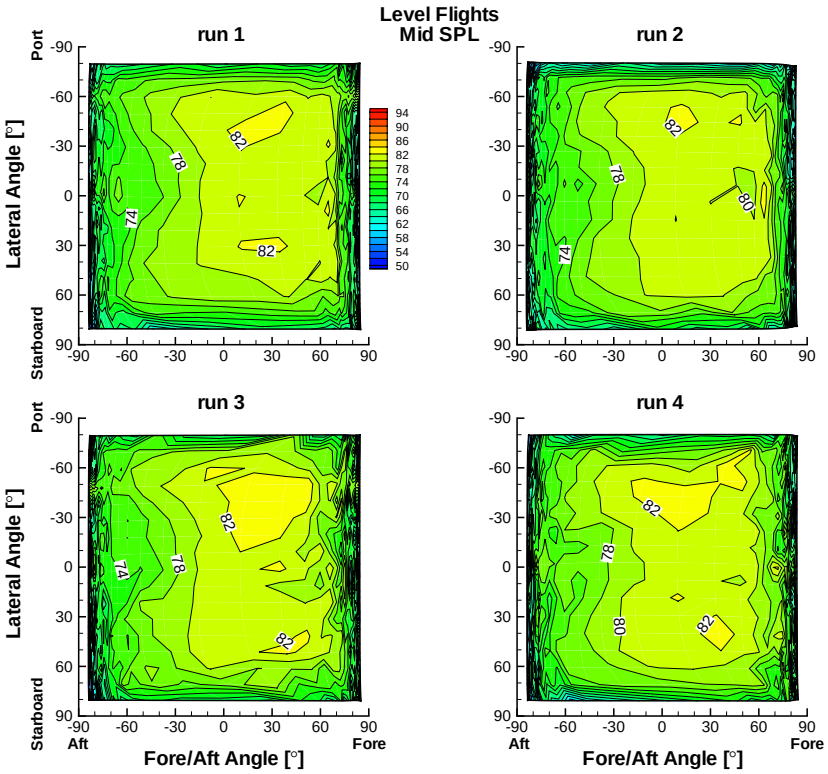

Figure 28: MidSPL contours for level flights.

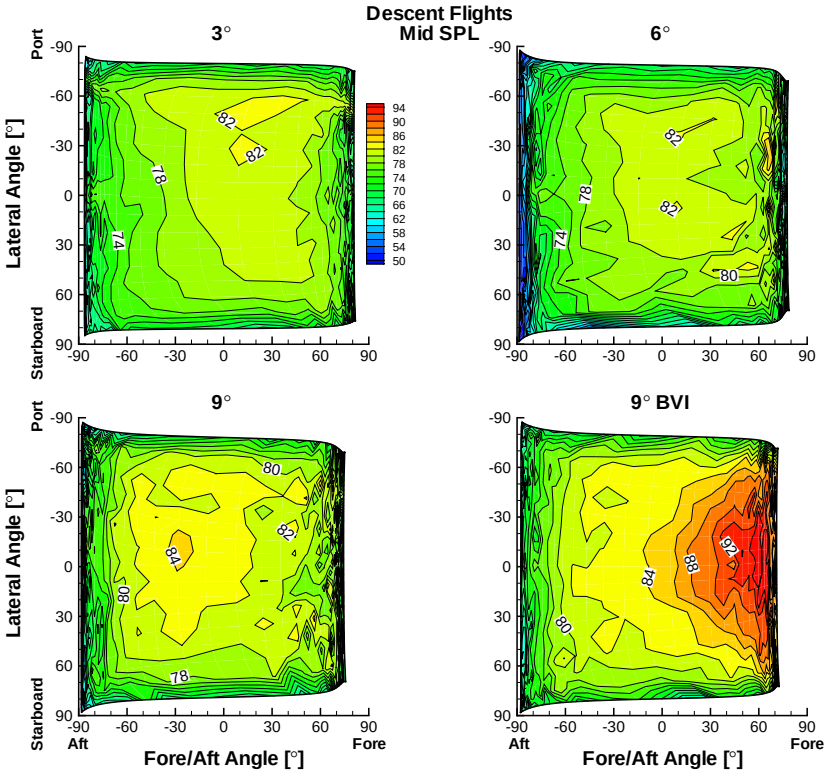

Figure 29: MidSPL contours for descent flights.

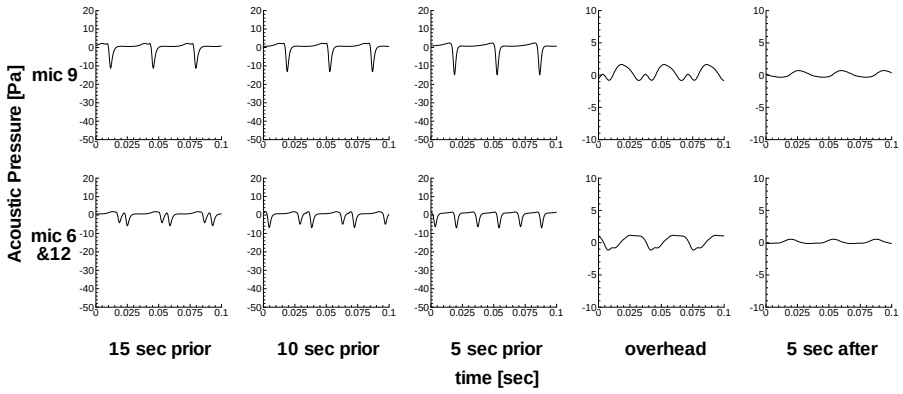

Figure 30: Prediction One acoustic pressure time histories (normalized) for centerline and sideline microphones for level flight conditions, time is relative to the aircraft overhead of the microphone array.

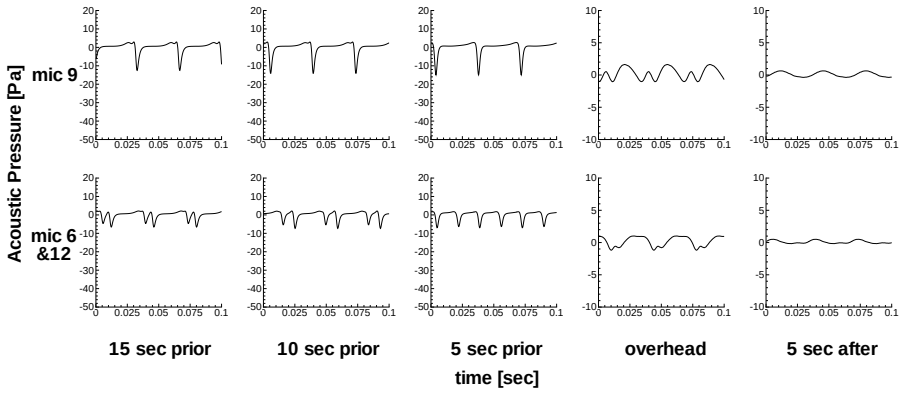

Figure 31: Prediction One acoustic pressure time histories (normalized) for centerline and sideline microphones for 3˚ descent condition, time is relative to the aircraft overhead of the microphone array.

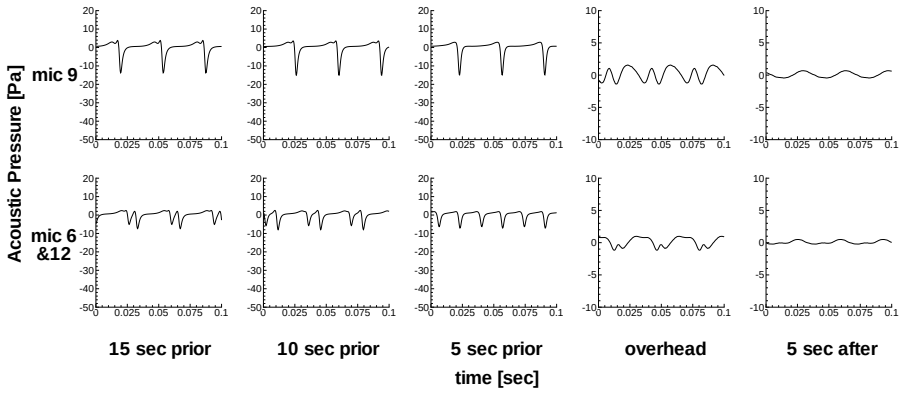

Figure 32: Prediction One acoustic pressure time histories (normalized) for centerline and sideline microphones for 6˚ descent condition, time is relative to the aircraft overhead of the microphone array.

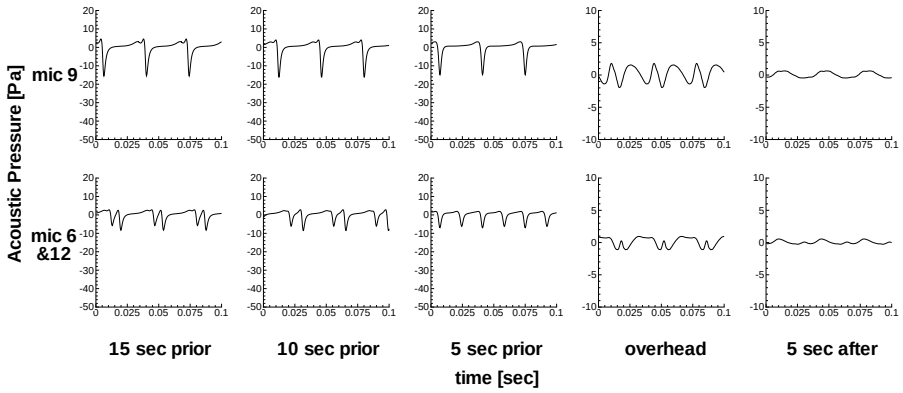

Figure 33: Prediction One acoustic pressure time histories (normalized) for centerline and sideline microphones for 9˚ descent condition, time is relative to the aircraft overhead of the microphone array.

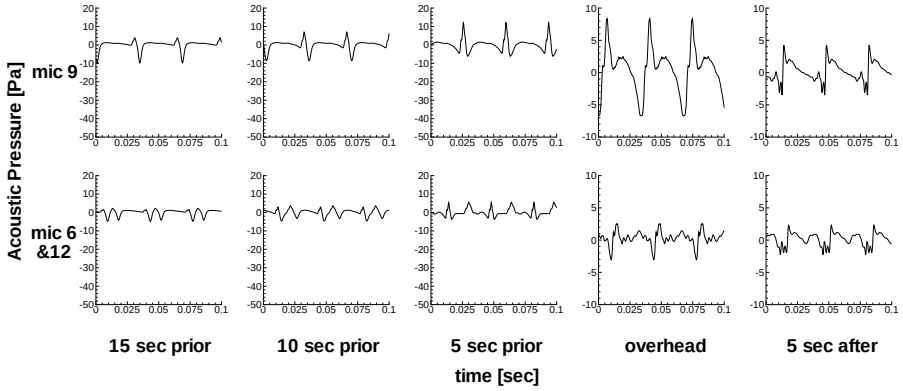

Figure 34: Prediction One acoustic pressure time histories (normalized) for centerline and sideline microphones for 9˚ descent BVI condition, time is relative to the aircraft overhead of the microphone array.

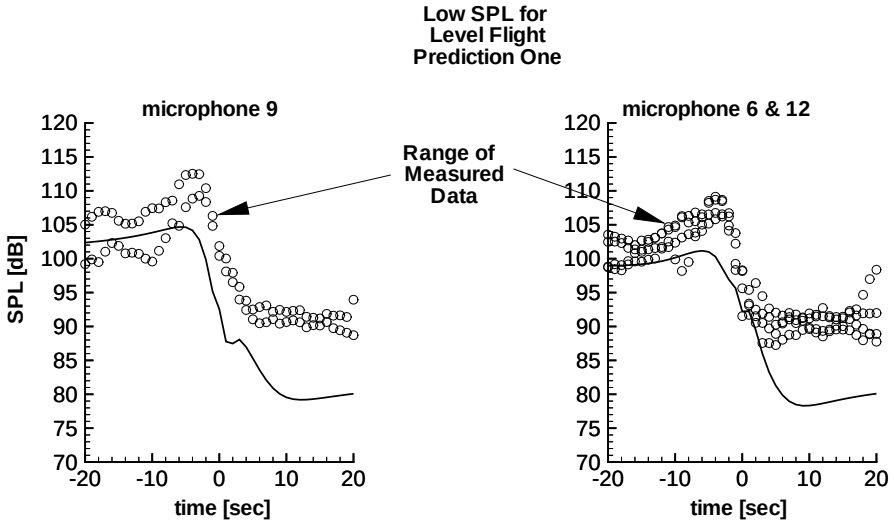

Figure 35: Prediction One LowSPL time histories for level flight (the aircraft is overhead at t= 0).

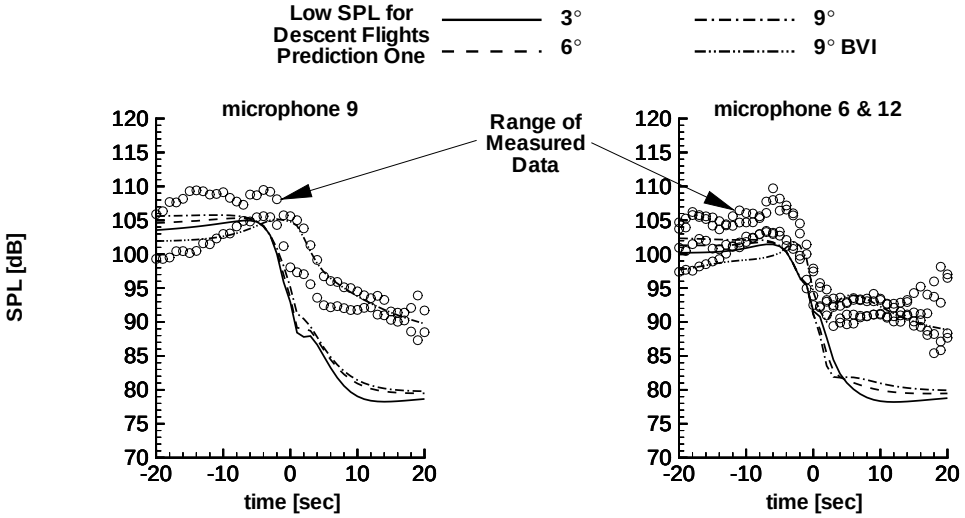

Figure 36: Prediction One LowSPL time histories for descent flights (the aircraft is overhead at t= 0).

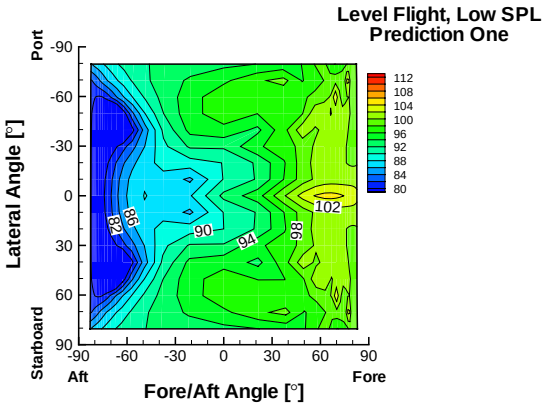

Figure 37: Prediction One LowSPL contours for level flight.

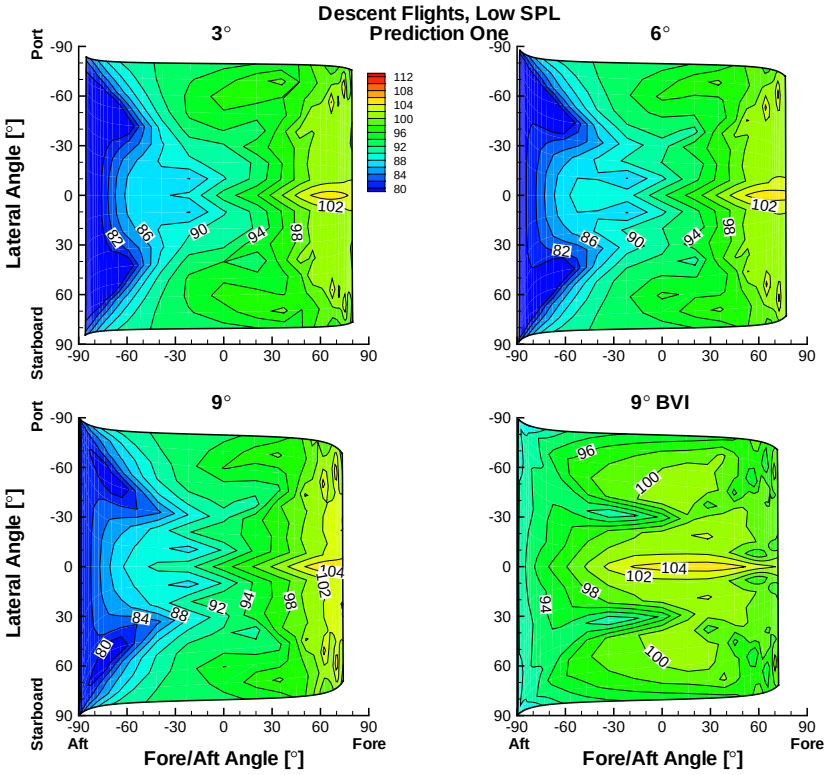

Figure 38: Prediction One LowSPL contours for descent flights.

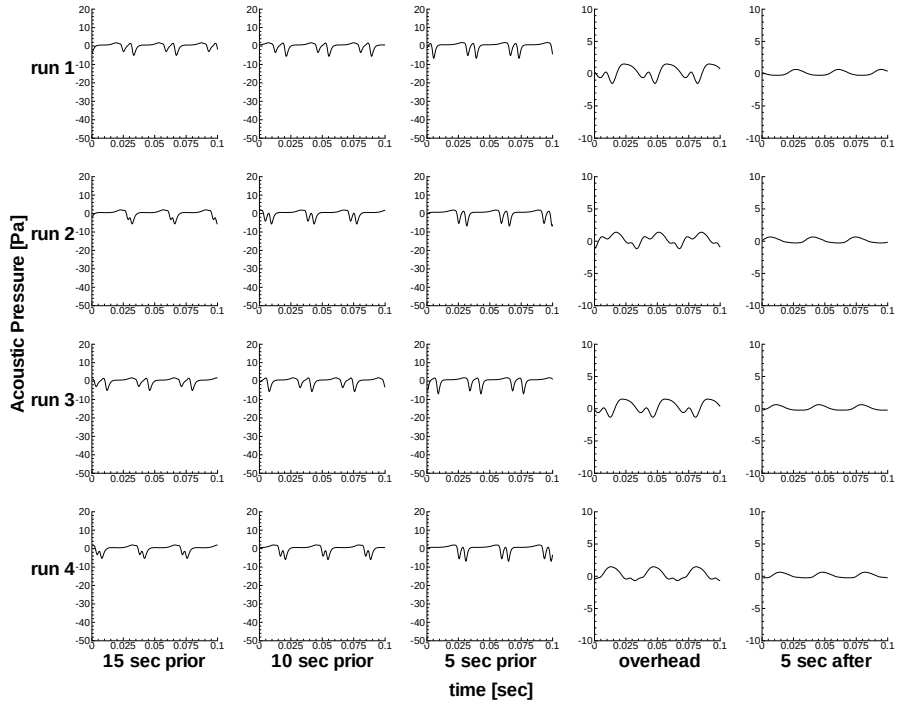

Figure 39: Prediction Two acoustic pressure time histories (normalized) for the centerline microphone 9 for level flight conditions, time is relative to the aircraft overhead of the microphone array.

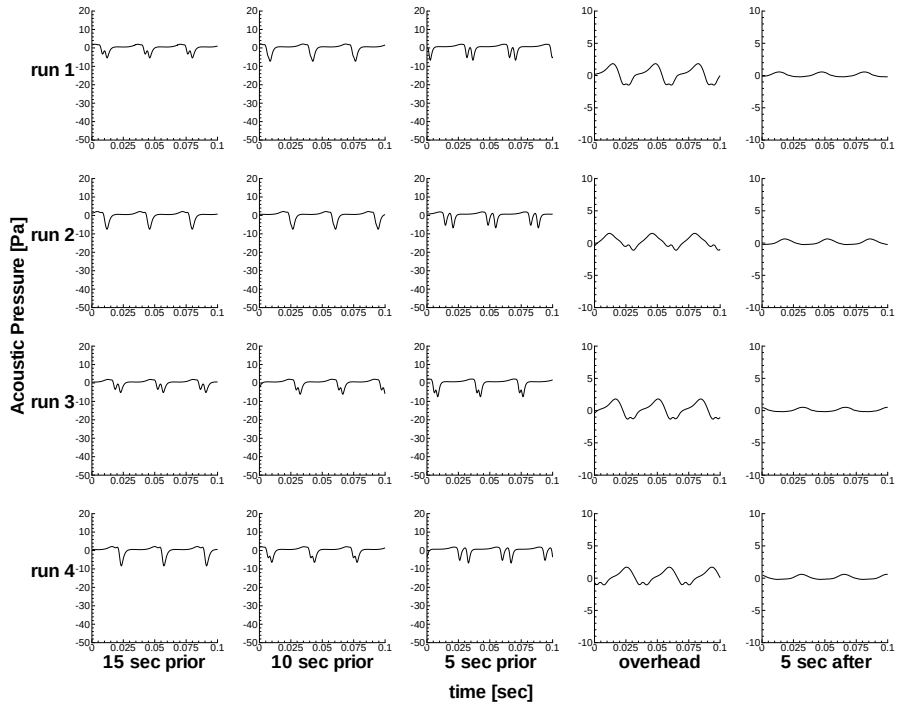

Figure 40: Prediction Two acoustic pressure time histories (normalized) for the starboard sideline microphone 6 for level flight conditions, time is relative to the aircraft overhead of the microphone array.

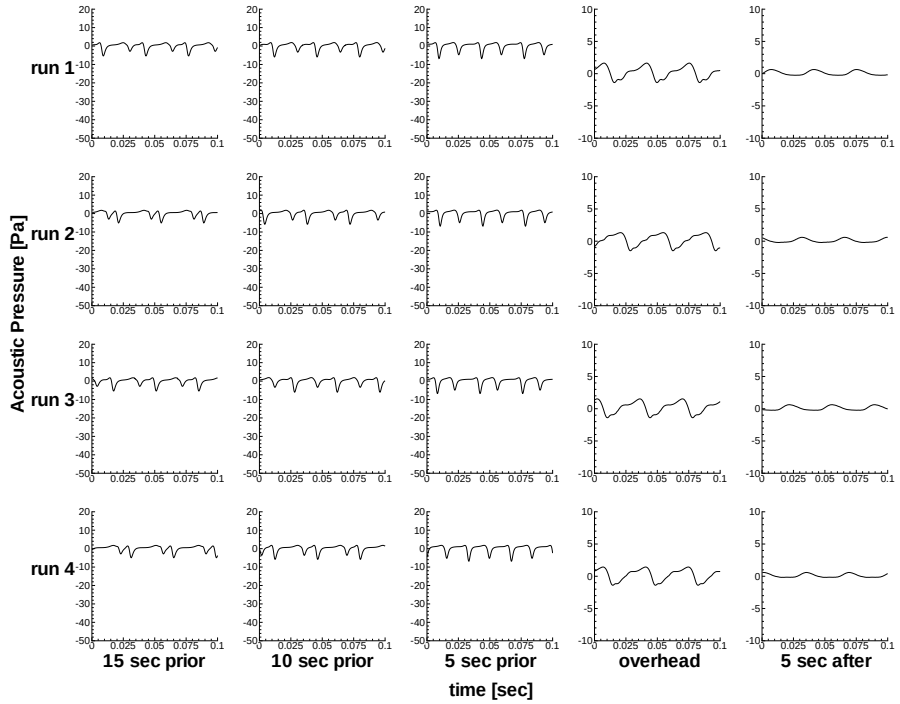

Figure 41: Prediction Two acoustic pressure time histories (normalized) for the port sideline microphone 12 for level flight conditions, time is relative to the aircraft overhead of the microphone array.

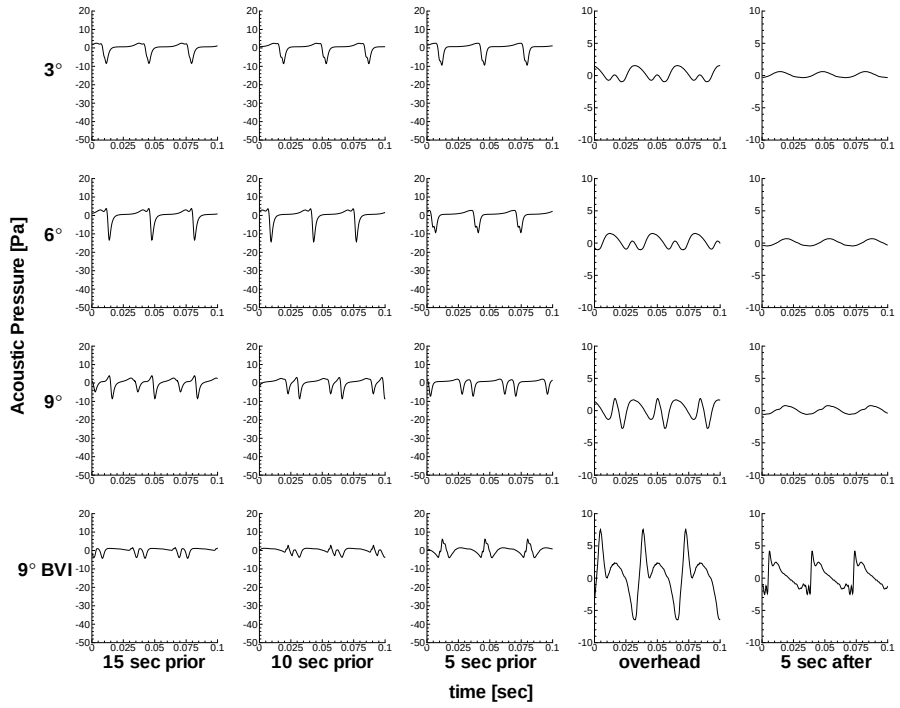

Figure 42: Prediction Two acoustic pressure time histories (normalized) for the centerline microphone 9 for descent flight conditions, time is relative to the aircraft overhead of the microphone array.

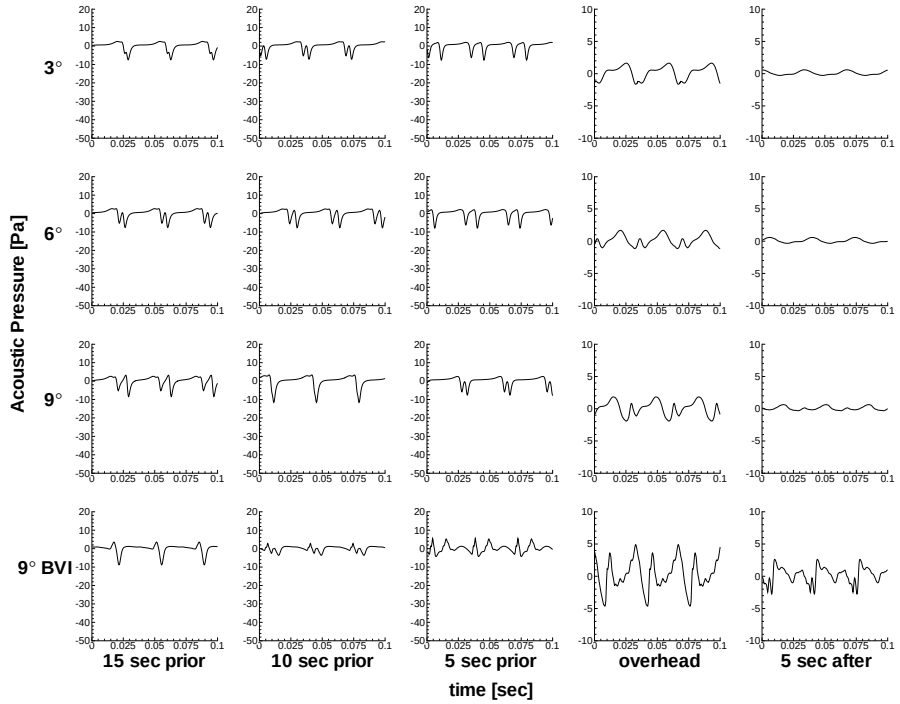

Figure 43: Prediction Two acoustic pressure time histories (normalized) for the starboard sideline microphone 6 for descent flight conditions, time is relative to the aircraft overhead of the microphone array.

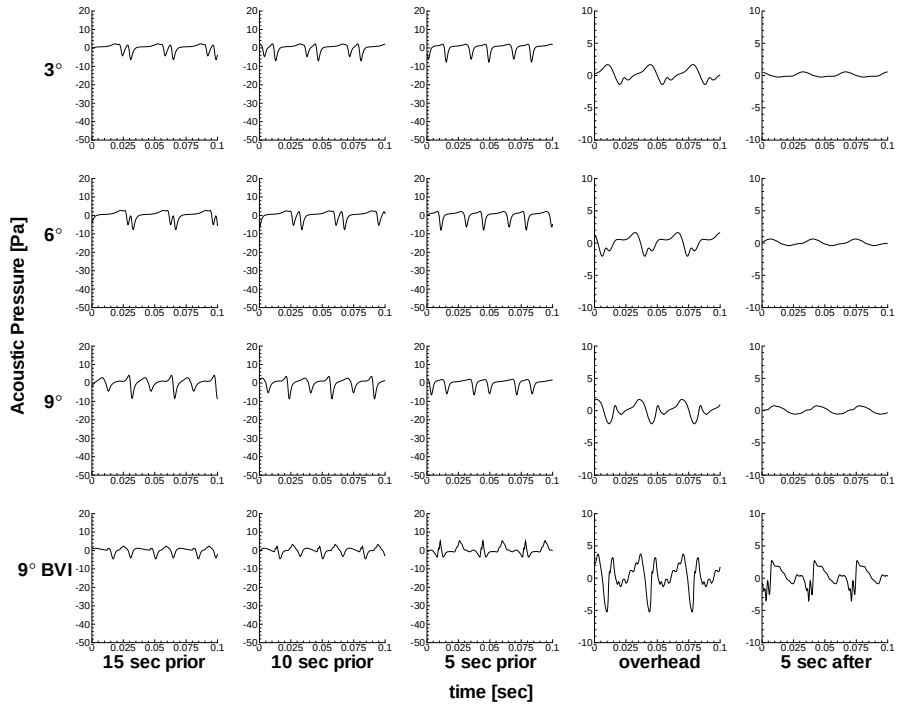

Figure 44: Predictions Two acoustic pressure time histories (normalized) for the port sideline microphone 12 for descent flight conditions, time is relative to the aircraft overhead of the microphone array.

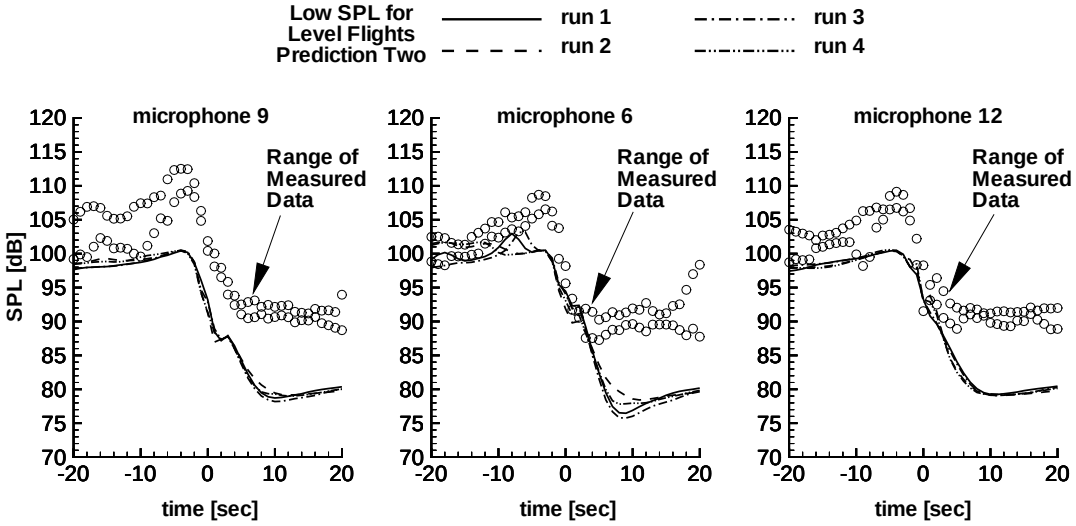

Figure 45: Prediction Two LowSPL time histories for level flights (the aircraft is overhead at t= 0).

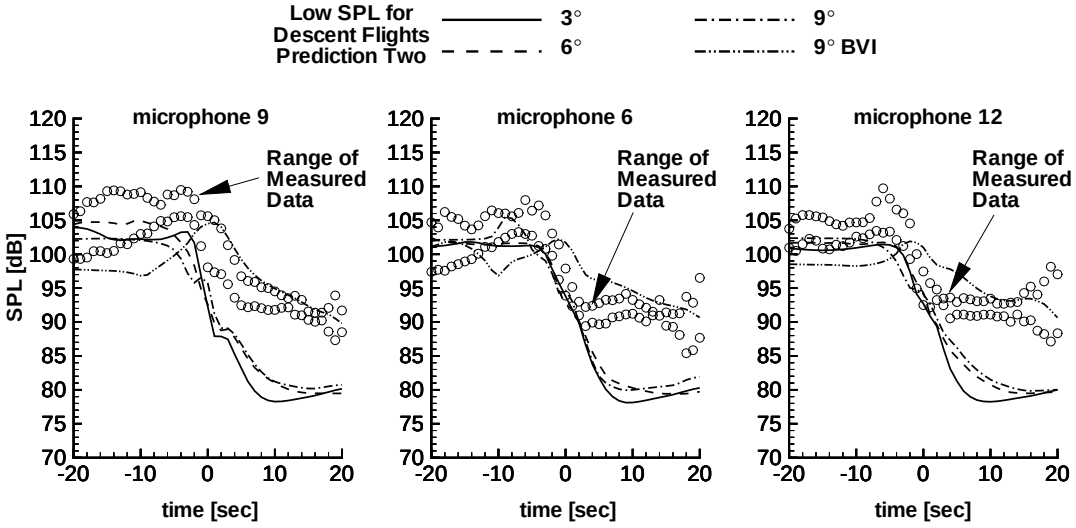

Figure 46: Prediction Two LowSPL time histories for descent flights (the aircraft is overhead at t= 0).

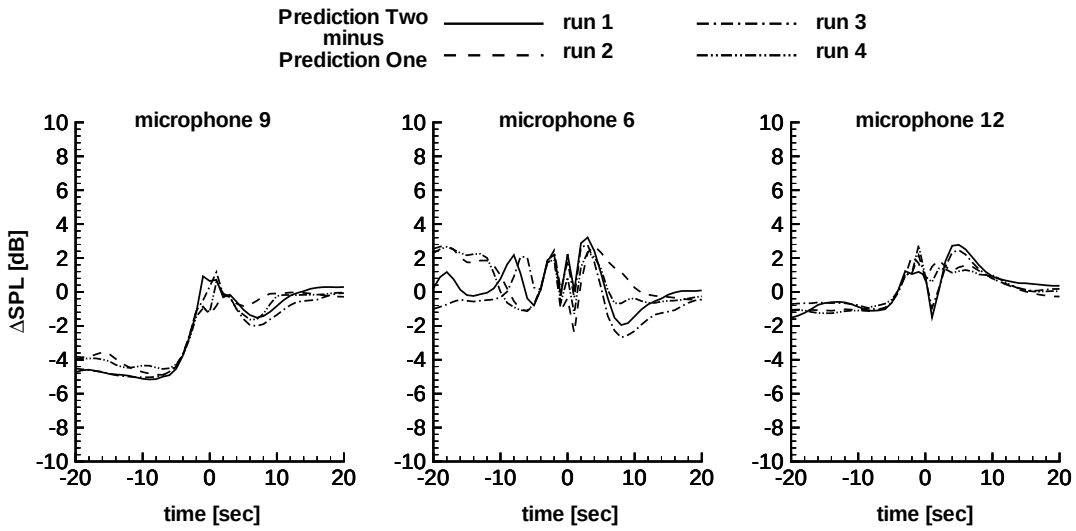

Figure 47: Difference Between Prediction Two and Prediction One for level flights (the aircraft is overhead at t= 0).

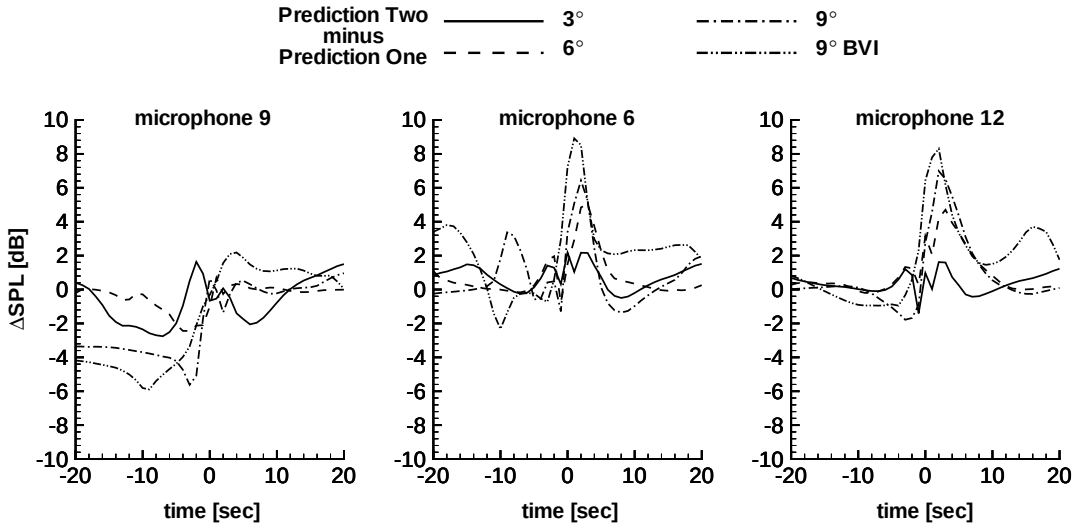

Figure 48: Difference Between Prediction Two and Prediction One for descent flights (the aircraft is overhead at t= 0).

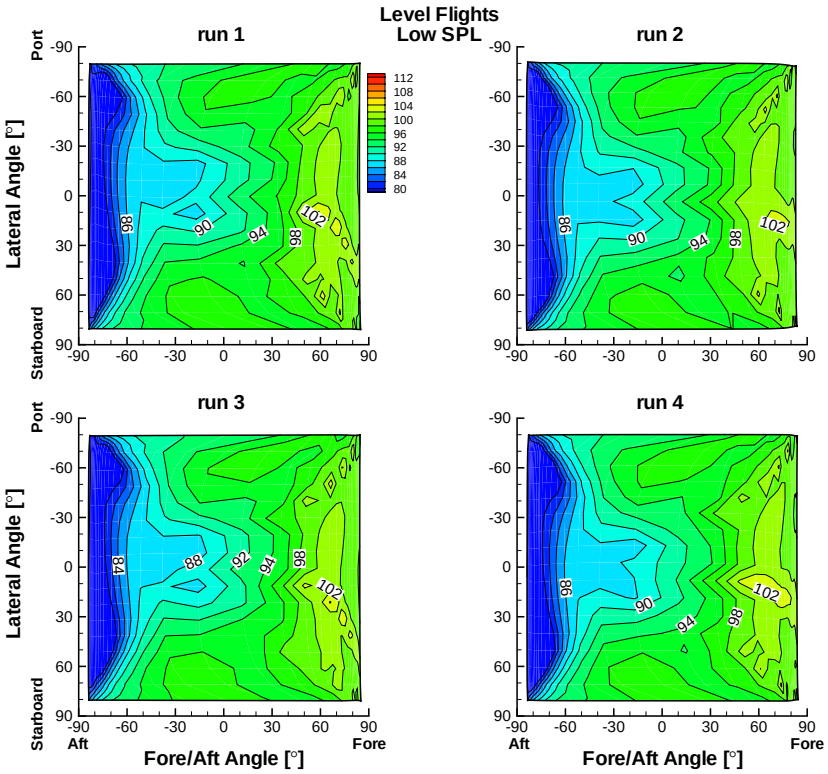

Figure 49: Prediction Two LowSPL contours for level flights.

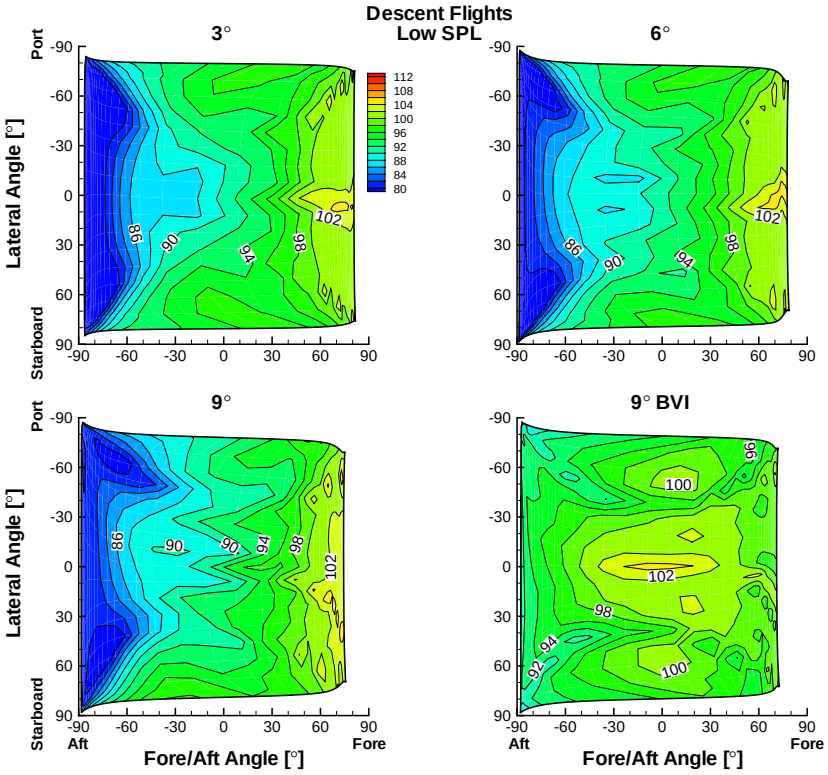

Figure 50: Prediction Two LowSPL contours for descent flights.